공학박사학위논문

Electron/ion-conductive Polymer Binders for Lithium-ion Batteries: Poly(phenanthrenequinone) and Poly(acrylic acid) Lithium Salt

리튬 이온 전지용 전자/이온 전도성 고분자 바인더: 폴리페난트렌퀴논 및 폴리아크릴산 리튬염

2016년 8월

서울대학교 대학원

화학생물공학부

김 상 모

Abstract

Electron/ion-conductive Polymer Binders for Lithium-ion Batteries: Poly(phenanthrenequinone) and Poly(acrylic acid) Lithium Salt

Sang-Mo Kim
School of Chemical and Biological Engineering
The Graduate School
Seoul National University

Among the components comprising a lithium-ion battery (LIB), the binder is a compound that binds mechanically the active material, the conductive additive, and the current collector, by which electrochemical reactions are well occurred in the electrode. As a conventional binder for LIBs, polyvinylidene fluoride (PVDF) has been widely used due to its superior chemical and electrochemical stability. According to that the researches regarding the active materials for higher capacity and higher power have been attracted attention, researches on the functional binders that can support the performances of them have been also conducted. In this study, electronic or ionic conductive polymer binders for high capacity silicon (Si) negative electrode and high power $LiFePO_4$ positive electrode are characterized electrochemically.

Si has been attracted much attention as an advanced negative active material due to its higher theoretical capacity (3579 mA h g^{-1}) than conventional

graphite. However, because Si experiences huge volume changes during charge-discharge, adhesive polymers such as carboxymethyl cellulose (CMC) and poly(acrylic acid) (PAA) have been considered to be used as alternate of PVDF binder having poor adhesion strength. In addition, nano-sizing of Si particles is a one of good strategy for achieving good cycle performance because absolute volume change of nano-sized Si is smaller than that of bigger Si particles. But, due to its high surface area, there is a problem about particle dispersion in slurry mixing process and high amount of conductive additive and polymer binder should be loaded to ensure the electrical network of the electrode. This brings lowered energy density of the electrode, especially volumetric energy density.

To this end, in the first subject of the first part (chapter 2.1), a new conductive polymer binder 3,6-poly(phenanthrenequinone) (PPQ) based on 9,10-phenanthrenequinone is developed and the function as a conductive additive is tested. The PPQ conductive binder becomes an electronic conductor at the first lithiation reaction (n-type doping) and maintains the conductive nature in the reaction voltage range of Si. Nano-sized- Si electrodes prepared without the conventional conductive additive shows superior rate capability compared to the electrode prepared with the non-conductive polymer binder. The internal resistance, measured using intermittent titration technique (GITT), of the electrode prepared with the PPQ conductive polymer binder is smaller than the electrode with non-conductive binder in both lithiation and de-lithiation periods. This is due to the developed electron pathways between the nano-Si particles or between the Si particle and the copper current collector by the PPQ conductive binder that is uniformly dispersed within the electrode. In other words, the PPQ binder plays a role of a conductive additive in the electrode. Due to this feature of the PPQ conductive binder, the loading of the PPQ

binder can be minimized down to 10 wt.% with reasonable cycle performance.

Although nano-sized Si powder has been researched for a promising negative active material, it has some problems such as low dispersion in slurry mixing and low tap density due to its high surface area and inter-particle repulsion. As a solution of this, using of micrometer-sized Si particles can be considered. In the second subject of the first part (chapter 2.2), for an application of submicrometer-sized Si powder prepared by ball-milling, an adhesive polymer, poly(acrylic acid) (PAA), is blended to the electrode with the PPQ conductive polymer binder. While the adhesion strength of the electrode prepared with only the PPQ binder is marginal as 0.06 N cm^{-1}, the electrode prepared to which 20 wt. % PAA to the total electrode weight was added showed 30 times high adhesion strength (~2 N cm^{-1}). This implies that the PPQ and the PAA binder play roles of a conductive additive and a material providing mechanical integrity of the electrode by its high adhesive property, respectively.

In the second part (chapter 3), the effect of a Li^+ ion conductive polymer binder on the fast discharge of $LiFePO_4$ positive electrode was studied. Due to its stable structure, flat discharge voltage profile, and high theoretical capacity (170 mA h g^{-1}), $LiFePO_4$ has been used for a positive active material for the batteries of power tools or electric vehicles. In order to decrease polarization during charge and discharge at high current rate, nano-sizing of the particles and surface carbon coating have been tried. But, the polarization can be also occurred due to Li^+ ion transfer in the interface between the active material and the electrolyte. To confirm the effect of a Li^+ ion conductive binder, poly(acrylic acid) lithium salt (LiPAA), electrochemical properties of the $LiFePO_4$ electrodes with the binders is examined. Discharge capacities of the $LiFePO_4$ electrode prepared with the LiPAA binder at high current

rates are higher than the control, the electrode prepared with poly(acrylic acid) (PAA) binder. In addition, polarizations observed in each discharge voltage plateaus of the electrode with the LiPAA binder are smaller than the electrode with the PAA binder. The smaller polarization to Li^+ ion transfer is observed in the LiPAA film compared with the PAA film, which was measured with a galvanostatic polarization test of a Li metal|polymer film|Li metal symmetrical cell. Also, resistance in the charge transfer in the electrode with the LiPAA binder is smaller than the electrode with the PAA binder, which was measured with an electrochemical impedance test. These imply that Li^+ ion transfer in the interface between the active material and the electrolyte is assisted by the Li^+ ion conductive binder because of higher Li^+ affinity of carboxylate anion compared with carboxylic acid, so improved discharge rate capability property can be obtained.

……

Keywords: Lithium-ion batteries, Electronic conductive binder, Li^+ ion conductive binder, Silicon negative electrode, $LiFePO_4$ positive electrode, Poly(phenanthrenequinone), Poly(acrylic acid).

Student number: 2010-31324

Contents

List of Figures

ratio).

Figure 11. Schematic representation of the nano-Si electrode fabricated without and with the conductive carbon.

Figure 12. (a) The charge-discharge voltage profiles of the Li/PPQ cell in the initial two cycles. (b) AC impedance results of the Li/PPQ cell, which is measured at OCV, after first lithiation and de-lithiation, and second lithiation.

Figure 13. The magnified view of the first differential capacity plots in the lithiation period of Li/nano-Si cells and Li/PPQ cell.

Figure 14. Rate capability of Li/nano-Si cells with two binders (30 wt.%). The de-lithiation current is indicated. For the lithiation, a constant current mode was used at 0.1 C.

Figure 15. Discharge voltage profiles of Li/nano-Si cells fabricated with (a) LiPAA and (b) PPQ binder. The de-lithiation currents are 0.1, 0.5, 1, 2, and 3 C, respectively.

Figure 16. (a) The transient voltage profiles obtained from the galvanostatic intermittent titration technique (GITT) and (b) the evolution of internal resistance derived from the difference between the end of closed-circuit-voltage (CCV) and the quasi-open-circuit voltage (QOCV). The GITT experiment was carried out after two charge-discharge cycles (pre-cycling).

Figure 17. Evolution of internal resistance below 0.2 V QOCV during lithiation (magnified view of Figure 16b).

Figure 18. (a) AC impedance spectra of Li/nano-Si cells fabricated with two binders and (b) fitting results by inset equivalent circuit. The The measurements were made at 0.5 V after third lithiation. Before the measurements, the cells were de-lithiated to

0.5 V and OCV of the cells allowed to maintain 0.5 V by constant-voltage de-lithiation.

Figure 19. TEM images of the nano-Si/polymer binder composites: (a–d) LiPAA and (e–h) PPQ. The bright-field STEM images and their EDS maps: (b–d) LiPAA and (f–h) PPQ. The red and green dots represent C and Si, respectively.

Figure 20. Schematic representation of electron conduction between the nano-Si particles covered with (a) LiPAA and (b) PPQ binder during lithiation and de-lithiation.

Figure 21. Cycle performance of Li/nano-Si cells (pre-cycling data are excluded). Specific capacity is calculated based on the weight of nano-Si, the active material (a) and total weight of the electrode (b). De-lithiation capacity is only displayed.

Figure 22. Coulombic efficiency of Li/nano-Si cells. Data at pre-cycling are included.

Figure 23. Electron conduction pathways in various nano-Si composite electrodes. (a) Without conducting agent: particle-to-particle or particle-to-current collector contacts. (b) With particulate conducting agent: enhanced electrical contacts but still remained disconnections. (c) Conducting binder: electrons can freely move within the electrode.

Figure 24. FE-SEM images of (a) pristine Si powder (1–5 μm), (b) ball-milled Si powder (submicrometer-sized). X-ray diffraction patterns of the powders (c). The ball-milling condition is 600 rpm for 30 min at Ar atmosphere.

Figure 25. (a) Cycle performance of the Li/Si cell with PPQ conductive binder without conductive additive, (b) the charge/discharge voltage profiles of Li/SM-Si

cell at first two pre-cycle. The binder content in the Si electrode is 30 wt.%.

Figure 26. Adhesion strength of the SM-Si electrodes with PPQ-PAA composite binder to the Cu current collector measured by the peel test. Sample name QAxy represents the Si electrode with the PPQ-PAA composite binder with blending ratio x:y. Peel test condition: 30 mm min^{-1}.

Figure 27. Cycle performance of Li/SM-Si cell with various composite binder (pre-cycling data are excluded) without conductive additive. The binder content in the Si electrode is 30 wt.%. Sample name QAxy represents the Si electrode with the PPQ-PAA composite binder with blending ratio x:y.

Figure 28. The voltage profile of Li/sm-Si cells at 1st, 5th, and 15th cycle with PPQ-PAA composite binder blended in ratio (a) 2:1, (b) 1:1 and (c) 1:2.

Figure 29. Differential capacity plots of the charge-discharge voltage profiles displayed in Figure 28.

Figure 30. The evolution of the internal resistance of the lithiated electrodes with the composite binders at each cycle derived from difference between charge cut-off voltage (0.07 V) and quasi-open circuit-voltage (QOCV).

Figure 31. (a) Cycle performance of Li/SM-Si cell with PPQ-PAA (2:1) composite and PAA binder without conductive additive, (b) the corresponding adhesion strength of the Si electrodes with PPQ-PAA (2:1) composite and PAA binder to the Cu current collector measured by the peel test, (c) the evolution of internal resistance of the lithiated electrodes at each cycle derived from difference between charge cut-off voltage (0.07 V) and quasi-open circuit-voltage (QOCV). PAA (7:2:1) means the electrode with the composition of Si : super-P : PAA = 7 : 2 : 1 (by weight).

Figure 32. An example of charge-discharge voltage profiles of Li/$LiFePO_4$ cell at different current densities.[106]

Figure 33. (a) FE-SEM image of $LiFePO_4$ powder, (b) TEM image of a carbon-coated $LiFePO_4$ particle, thickness of the carbon layer is around 10 nm, (c) XRD pattern of $LiFePO_4$ powder.

Figure 34. FT-IR spectra of (a) PAA film and (b) LiPAA film coated on a piece of Al foil, respectively. To confirm the possibility of change of carboxylic acid of PAA to carboxylic acid Li salt, spectra of the PAA film electrodes that were stored in the electrolyte or cycled via cyclic voltammetry were also obtained.

Figure 35. (a) The charge-discharge cycle performances of Li/$LiFePO_4$ cells (pre-cycling data are excluded), in which the working electrodes are fabricated with the PAA and LiPAA binder and the voltage profiles at the first cycle (b) and the fortieth cycle.

Figure 36. The charge-discharge voltage profiles of Li/$LiFePO_4$ cells in which the $LiFePO_4$ electrode fabricated with PAA binder (a) and LiPAA binder (b). (c) Polarization at each discharge rate is calculated with the difference between quasi-open-circuit voltage at discharge plateau and discharge voltage plateaus (closed-circuit voltage).

Figure 37. Potentiostatic polarization of Li/$LiFePO_4$ cells. (a) Experimental concept and (b) current behavior during potential step.

Figure 38. Galvanostatic polarization of Li/binder film/Li symmetrical cell. (a) Concept of the experiment and polarization behavior of the cells with PAA film (b) and LiPAA film (c). Thickness of the films is 70–80 μm.

List of Tables

1. Background

1.1 Principles of electrochemical cells

Batteries are devices that provide electrical power to machines such as clocks, toys, or cars. The term “battery” is a so-called name and has been referred to a devices consisting of single or multiple “electrochemical cells”. In an electrochemical cell, basically, electrical energy is generated from chemical energy of the active materials by electrochemical reduction and oxidation reactions. The electrochemical reaction involves moving of electrons between reactants and products. The oxidation reaction is the process of losing electrons from a chemical, then moving to the electrode. On the contrary to this, the reduction reaction is moving of electrons released from a chemical. An example of the oxidation and reduction reaction is described as follows:

$$Fe^{2+} \rightarrow Fe^{3+} + e \quad \text{(oxidation reaction)}$$

$$Cu^{2+} + 2e \rightarrow \mathrm{Cu} \quad \text{(reduction reaction)}$$

For construction of an electrochemical cell, two half-cells are need. When oxidation reaction occurs in one half-cell, reduction reaction should be occurred in the other half-cell. According to whether the electrochemical reaction is spontaneous or not, the electrochemical cells fall into two categories: electrolytic cell and Galvanic cell. If the variation of standard Gibbs free energy (ΔG^0) of the total reaction is positive, external energy should be provided into the cell because of its non-spontaneity. Electrolysis of salt water (NaCl solution) for production of NaOH

and Cl_2 gas is in the case of electrolytic cell. On the other hand, batteries are a kind of electrochemical cells with spontaneous reaction in which the variation of standard Gibbs free energy of the total reaction is negative. Generally, a galvanic cell is consisted of anode, cathode, and electrolyte. Electrochemical oxidation and reduction reaction are occurred in anode and cathode, respectively. Electrons are released from the anode and are delivered to external electrical circuit, then injected to the cathode. At the same time, ions in the electrolyte take part in the delivery of charges. Anodic and cathodic current, current by the electrolyte should be same. To establish the closed loop, whole process should be occurred simultaneously. A general representation of electrochemical redox reaction in galvanic cell is described as follows:

$$\text{Anode: } \nu_A A \rightarrow \nu_C C + ne \text{ (oxidation reaction) (1a)}$$

$$\text{Cathode: } \nu_B B + ne \rightarrow \nu_D D \text{ (reduction reaction) (1b)}$$

$$\text{Overall: } \nu_A A + \nu_B B \rightarrow \nu_C C + \nu_D D \ (\Delta G^0 < 0) \text{ (1c)}$$

where *A*, *B*, *C* and *D* are chemical species involved in the electrochemical reactions, ν_A, ν_B, ν_C, and ν_D are moles of chemical species involved in the electrochemical reactions, and *n* is moles of electrons involved in the electrochemical reactions.

At standard state (activity of the species is 1), electromotive force is measured by difference between the two half-cells and relationship between the variation of Gibbs free energy and the electromotive force is described as follows:

$$\Delta G^0 = -nFE^0$$

where *n* is moles of electrons involved in the reaction, *F* is Faraday constant (9.6485

$\times 10^4$ *equiv.*$^{-1}$), and E^0 is standard electromotive force (V).

On the other hand, in non-standard state, activity of the chemical species except solid or metal whose activity is constant is considered to derive the equilibrium potential (E_{eq}) as follows:

$$E_{eq} = E^0 + \frac{RT}{nF} ln \frac{a_A^{\nu_A} a_B^{\nu_B}}{a_C^{\nu_C} a_D^{\nu_D}}$$

where a_i is activity of species i, R is gas constant (8.314 J K^{-1} mol^{-1}), and T is absolute temperature (K).

In the electrochemical cell with the reaction of 1a–1c, if the system is reversible, reverse reaction can be occurred when external energy is supplied to the cell. In the case of the reaction 1a, reduction reaction is now occurred in the electrode in which oxidation reaction was occurred (switched from Galvanic cell to electrolytic cell). Name of the electrode is changed from anode to cathode. Rechargeable battery is in the case while primary battery is Galvanic cell. So, instead, the term "positive electrode" and "negative electrode" are recommended. The electrode with higher electron energy (lower electrical potential) is negative electrode and the electrode with lower electron energy (higher electrical potential) is positive electrode.

1.2 Development of lithium-ion batteries

Rechargeable batteries are one kind of batteries which can be re-used after being discharged by re-charging while primary batteries are discarded after single discharging. Primary batteries have been still used for consumer products such as

remote controller of electronic devices, toys, clocks, computer memories etc. and for special applications such as implantable cardiac pacemakers. However, the unique advantages of re-use of rechargeable batteries brings more various applications compared to the primary batteries.

As growing consumer applications market of portable devices such as mobile phone, laptop computers, digital cameras and camcorders, lithium-ion batteries have been highlighted as new power sources. The history of development of lithium-ion batteries goes back to the 1970s. Lithium secondary batteries with lithium intercalation mechanism were proposed by M. S. Whittingham (Exxon company) firstly.[1,2] Li metal was used as a negative electrode because Li provides high energy density due to its lowest standard reduction potential (−3.045 V (*vs*. NHE)) and lowest density among metals (0.534 g cm^{-3}). Transition metal chalcogenides such as titanium disulfide (TiS_2) were used as a positive electrode.[2,3] The practical use of lithium secondary batteries began with the Li metal/MoO_2 in the late 1970s, early 1980 period introduced by Moli Energy. Unfortunately, development of the batteries with Li/MoS_2 was not continued because of safety problem with lithium metal use. The main reasons of the fail were lithium dendrite growth to positive electrode during coupled charge-discharge and resulted short-circuit and explosion of the cell. In the late 1980s, negative electrode material with intercalation mechanism was proposed and this technology was called lithium-ion or rocking-chair. In this material, growth problem of lithium dendrite was not shown and safety of the cells was drastically improved.[4,5] Schematic representation of the cells with lithium metal and rocking-chair technology is showed in Figure 1. Commercialization of the lithium secondary batteries with rocking-chair technology was realized by Sony Energytech in Japan thanks to the development of highly reversible lithium storage in carbon based negative electrode. Since Sony named the

lithium secondary batteries “lithium-ion battery (LIB)” in 1991, LIB became a common name of the lithium rechargeable batteries with intercalation (or insertion) mechanism.[6-8] As positive electrode materials, lithium metal oxides have been used since Li_xMO_2 (M = Co, Ni, Mn) were introduced by J. B. Goodenough and coworkers in late 1970s.[9-11]

1.3 Basic cell design and principles of operation

Typical structure of unit cell of lithium-ion batteries is depicted in Figure 2. Commercialized active materials for lithium-ion batteries are intercalation type materials. For the negative electrodes and the positive electrodes, graphite and layered lithium metal oxides are widely used. Generally, the composite electrodes are fabricated by coating a mixture of active material powder, conductive additive (carbon black), polymeric binder (polyvinylidene fluoride, PVDF), and *N*-methyl-2-pyrrolidone (NMP, solvent) on a current collector (copper foil for the negative electrode, aluminum foil for the positive electrode). Separator has an important role of preventing electronic contact between the negative electrode and the positive electrode. To ensure free ionic transport across the cell, the separator must have proper porosity to hold sufficient amount of liquid electrolyte. It is also important that permeability of the separator must be uniform to prevent dendrite growth due to non-uniform current distribution. Supporting electrolyte generally used in the batteries is solution of lithium hexafluorophosphate ($LiPF_6$) in aprotic carbonate solvents (ethylene carbonate, dimethyl carbonate etc.). The electrochemical reactions of the cell with graphite/$LiCoO_2$ configuration are as follows:

Positive electrode: $LiCoO_2 \rightleftarrows Li_{1-x}CoO_2 + xLi^+ + xe$

Negative electrode: $xLi^+ + xe + 6C \rightleftarrows Li_xC_6$

Lithium ions move from the $LiCoO_2$ positive electrode (oxidation) to the graphite negative electrode (reduction) during charge. During the initial cycles, solid electrolyte interphase (SEI) is formed due to the reduction of the organic electrolyte. Because electrons are not able to across the SEI, additional charge consumption by the electrolyte degradation is hindered on the surface of graphite.[12-15] Lithium ions move backward and during discharge. Thus, technology of lithium-ion batteries with insertion (or intercalation) type active material is called “rocking chair”.

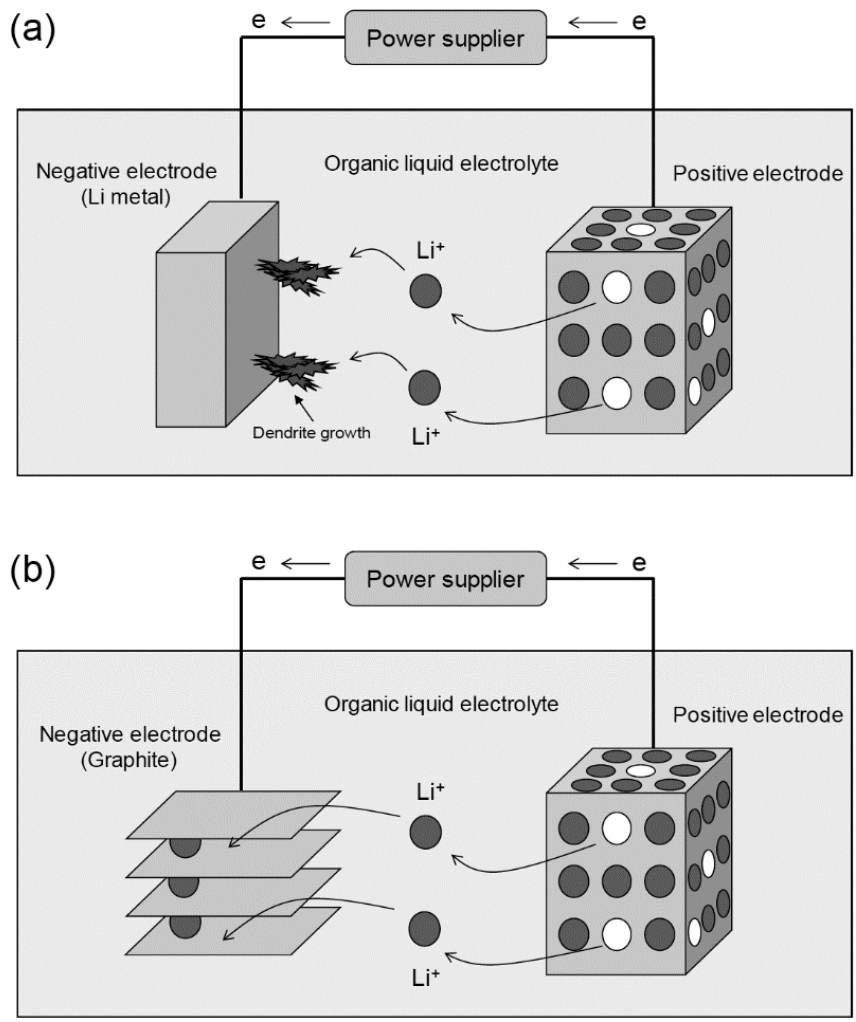

Figure 1. Schematic diagram of lithium rechargeable battery with negative electrode, (a) Li metal, (b) intercalation type material (graphite).

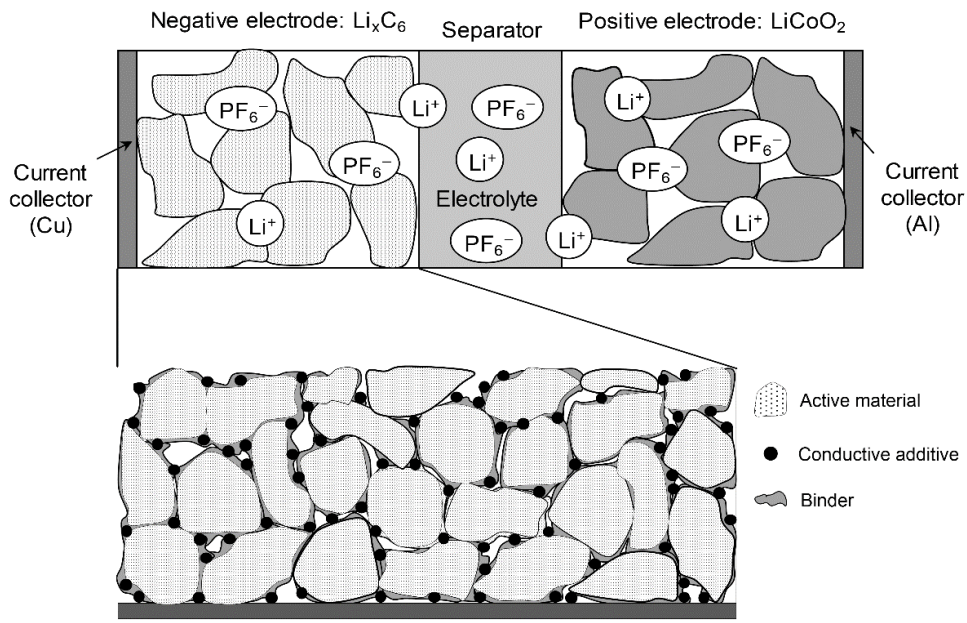

Figure 2. Basic design of lithium-ion battery and electrode components.

1.4 Materials in the lithium-ion batteries

1.4.1 Positive electrode materials

$LiCoO_2$ which is most widely used positive active material for lithium-ion batteries is firstly introduced in 1980 by J. B. Goodenough. Working voltage of $LiCoO_2$ is around 4 V (vs. Li/Li^+). However, because of limited stability of the electrolyte at that time, $LiCoO_2$ did not get much attention. With improvement in the stability of the organic electrolyte, SONY commercialized lithium-ion batteries in 1991 and $LiCoO_2$ has been used for the representative positive electrode material. After successful introduction of $LiCoO_2$, researches about the alternative positive active materials with higher energy density have been conducted extensively. To increase the capacity, nickel-based materials such as $LiNiO_2$ were investigate. However, several issues about difficulties in the synthesis and thermal instability at charged state (de-lithated) make practical use be hard. To overcome these problems, doping of cobalt and aluminum has been considered. For more stable structure and lower cost, researches about spinel $LiMn_2O_4$ or olivine $LiFePO_4$ have been conducted.

1.4.2 Layered transition metal oxides

Layered lithium transition metal oxides $LiMO_2$ (M = Co, Ni, Mn, etc.) have been investigated as positive electrode materials for lithium-ion batteries. Among layered transition metal oxides, $LiCoO_2$ was firstly commercialized and is still observed

today in the lithium-ion batteries. $LiCoO_2$ has a structure of rhombohedral α-$NaFeO_2$ or $CsCl_2I$ with distorted octahedrons. Cobalt and lithium are located in octahedral sites and occupy alternating layers of cubic close-packed arrangement. In a view of unit cell, lithium is coordinated octahedrally between CoO_6 layer. Electrochemical extraction of whole lithium from $LiCoO_2$ (charge) corresponds to theoretical specific capacity of 274 mA h g^{-1}. In this condition, however, reversible lithium insertion is hindered due to formation of irreversible phase. If amount of lithium extraction is limited to half (x=0.5, in Li_xCoO_2, charged up to 4.2 V), reversible lithium insertion can be occurred and corresponding specific capacity is 137 mA h g^{-1}.[16-18] Although $LiCoO_2$ is mainly used, alternatives that have higher energy density and lower cost have been studied. Among the candidates, $LiNiO_2$ attracted attention because of its higher specific capacity (170–200 mA h g^{-1}) and lower cost. But, practical use of $LiNiO_2$ was not realized due to difficulties in the synthesis of high valence state of trivalent nickel (stoichiometric $LiNiO_2$) and low thermal stability at the high state-of-charge (SOC). In the synthesis procedure, lithium tends to be lost and some nickel (trivalent) is reduced to divalent nickel. As a result, divalent nickel moves to Li^+ 3a sites because size of Li^+ and Ni^{2+} is similar. This phenomenon is called "cation mixing effect". Poor electrochemical properties such as low first cycle reversibility result from nonstoichiometry of $Li_{1-x}Ni_{1+x}O_2$.[19] To improve the properties of $LiNiO_2$, doping with various cations such as Co, Mn and Al has been carried out. Among various modified $LiNiO_2$, $LiNi_{0.8}Co_{0.15}Al_{0.05}O_2$ (NCA) is successfully commercialized because of improved thermal stability and electrochemical properties.[20,21]

1.4.3 Spinel lithium-manganese oxides

Lithium-manganese spinel ($LiMn_2O_4$) is an attractive active material for the positive electrode of lithium-ion batteries. It is more environmental friendly, safer and cheaper than cobalt or nickel-based layered oxides. Due to its three-dimensional spinel structure, use of it is advantageous to the batteries with high rate capability. In lithium-manganese oxide spinel, lithium ions occupy tetrahedral 8a sites and manganese ions are located in octahedral 16d sites in a cubic close-packed array of oxygen anions. Lithium diffusion pathways are provided by interstitial tetrahedral and octahedral sites in the three-dimensional structure. Electrochemical extraction of lithium from $LiMn_2O_4$ to form λ-MnO_2 (plateau around 4 V versus Li/Li^+) delivers theoretical specific capacity of 148 mA h g^{-1}. Electrochemical insertion of lithium is also possible, during which voltage plateau around 3 V (*vs*. Li/Li^+) is observed, representing concurrent reduction of Mn and formation of tetragonally distorted phase $Li_2Mn_2O_4$ due to the Jahn-Teller effect. In this process, anisotropic change of lattice parameter (volume change) during the transition from cubic to tetragonal structure results in formation of defects in the microstructure. Thus, lithium insertion that is limited to the 4 V plateau is desirable. However, some problems for practical application of $LiMn_2O_4$ were observed, capacity fading during repetitive cycling or storage at high temperature.[22-25] These are related to the Jahn-Teller distortion, disproportionation of Mn^{3+}, dissolution of Mn^{2+} by HF attack, etc. To improve capacity retention, partial substitution of manganese by other elements such as cobalt, aluminum, magnesium, etc. was considered.[26-28] This creases the average valence state of manganese ion, thus, stability of the structure increased. For the stability in the high temperature condition, surface coating with compounds such as Al_2O_3 and

$AlPO_4$ was conducted.[29,30]

1.4.4 Phospho-olivines

As an another class of the positive active materials, phosphor-olivine structure was proposed in 1997 by Goodenough and coworkers.[31] $LiFePO_4$ is the most promising material because iron is one of the most abundant elements in the earth and it is cheaper and more environmentally friendly than cobalt. In the $LiFePO_4$ structure, lithium and iron ions occupy octahedral sites and phosphorous ions form hexagonal close-packed structure with oxygen atoms on tetrahedral sites. The FeO_6 and LiO_6 octahedra form zigzag corner-sharing chains and edge-sharing chains, respectively. Lithium ions can move through the one-dimensional tunnels that formed by the structure. Electrochemical lithium extraction and insertion are occurred at around 3.45 V (*vs*. Li/Li^+), which is contrast to the case of $LiFeO_2$ (3.2 V). This difference is originated from the fact that ionic character of P-O is increased (decreased in Fe-O) due to the inductive effect of P-O bond.[32] $LiFePO_4$ delivers theoretical capacity of 170 mA h g^{-1} and shows good thermal and chemical stability. Although many advantages are attractive, because electronic conductivity and lithium ion diffusion is poor, surface coating with carbon and down-sizing of particles to nano-scale were considered.[33-36] Due to its outstanding stability compared to conventional layered or spinel structure materials, $LiFePO_4$ has been adopted as a positive active material of lithium-ion batteries for vehicles for the transportation such as bus mainly in China.[37]

1.5 Negative electrode materials

For the negative electrode of the lithium secondary batteries with high energy density, low standard electrode potential and high gravimetric or volumetric capacity are needed because energy is determined by the product of voltage and capacity. In this view, lithium metal is the most promising as a negative electrode material because its standard electrode potential is lowest among the metals and highest gravimetric (3860 mA h g^{-1}) and volumetric capacity (2062 mA h cm^{-3}). As seen in the history, however, application of lithium metal was not trustful because of its poor cycle performance and safety due to uneven surface formation by repetitive dissolution and plating, which results in the generation of dead lithium or internal shot-circuit due to dendrite growth. Without solving these problems, lithium metal cannot be used for the negative electrode although it delivers extraordinary performances. Since the “rocking-chair” mechanism was proposed, researches and developments have been focused on carbonaceous material. In addition, for higher energy density, elements such as Si and tin that are electrochemically form alloys with lithium have been investigated.

1.5.1 Carbonaceous materials

Among the allotropes of the carbonaceous materials, carbons with sp^2 or mixture of sp^2 and sp^3 hybrid molecular orbitals show electrochemically reversible lithium insertion/extraction and have been used for the negative electrode materials for lithium-ion batteries. According to characteristics of the structure, the carbonaceous

materials are categorized into graphite and non-graphite. Since the carbonaceous materials were adopted for the negative electrode active materials, graphite has been mainly used. Graphite consists of layered hexagonal sheets with sp^2-carbons (graphene layer). Each layers are bound by weak van der Waals forces and are stacked alternatively by ABAB… sequencing along *c*-axis. Within the graphene layer, carbons are connected by strong covalent bonding. Surfaces which is parallel and perpendicular to c-axis are called the basal and edge planes, respectively. Lithium ions can be inserted (intercalation) and extracted (de-intercalation) between the layers.[38] Electrochemical intercalation is occurred below 0.25 V through edge planes until fully charged state LiC_6 is formed, which delivers theoretical capacity of 372 mA h g^{-1}. When the lithium ions are intercalated, voltage profiles showing several plateaus are observed. This is because that intercalation of lithium into the interlayer is two-phase reaction with several stages.[12,39,40] Meanwhile, non-graphite carbons have disordered structure compared to graphite and are divided into two classes of graphitizable carbon (or soft carbon) and nongraphitizable carbon (or hard carbon). By heat treatment above ~2200 °C, soft carbon can be graphitized while hard carbon cannot be graphitized even heat treat temperature exceeds 2800 °C. Turbostatic disordered structure is found in soft carbon when the heat treatment temperature is relatively low (< 1000 °C), which has some stacked structure but not with long range order. Electrochemical lithium intercalation is limited due to poor development of layered structure. Instead, lithium can be stored in cavities or defect sites.[41,42] Because of this structural characteristics, sloping voltage profiles are observed during lithium insertion and extraction.

1.5.2 Lithium alloys

Lithium-ion batteries have been occupied the market of energy storage for portable electronic devices, power tools, toys and so on. Although it took considerable efforts to improve the energy density of the lithium-ion batteries about three times (from 200 Wh L^{-1} in 1992 to 600 Wh L^{-1} in 2009, based on cylindrical 18650-type cell),[43] it is not enough to satisfy higher energy storage needs for the application of electric vehicle or energy storage system. Among the candidates except lithium metal that has safety issues, elements which electrochemically alloyed with lithium such as aluminum, silicon, tin, antimony, bismuth, magnesium, and zinc have been attracted much attention since 1960s.[44] These materials experience quite reversible alloying/de-alloying reaction. Among the alloying materials, silicon and tin are attractive and extensively investigated. Silicon and tin deliver much higher specific capacity of 3579 mA h g^{-1} and 994 mA h g^{-1}, respectively, than graphite (375 mA h g^{-1}). Most researches about alloying materials have been focused on silicon. Although silicon has been attracted much attention during last decades, commercialization of silicon powder as a negative material is difficult. This is due to its huge volume change (about 320 %, based on $Li_{22}Si_5$ phase) during charge and discharge cycling. Many researchers have been agreed that down-sizing to nanometer scale[45-48] and introduction of buffer matrix or hollow structure[49-56] to compensate the volume change. As another approach, using of more adhesive polymer binder than polyvinylidene fluoride conventional binder has been considered to be used for the conservation of the mechanical integrity of the electrode.

Table 1. Comparison of theoretical capacity and volume change of some alloying materials.

Elements	Li	C	Si	Sn	Al	Mg
Lithiated phase	Li	LiC_6	$Li_{22}Si_5$	$Li_{22}Sn_5$	LiAl	Li_3Mg
Theoretical gravimetric capacity (A h kg^{-1})	3862	372	4200	994	993	3350
Theoretical volumetric capacity (A h L^{-1})	2047	837	9786	7246	2681	4355
Volume change (%)	100	12	320	260	96	100

1.6 Binder

The binder plays an important role of mechanical binding together the active materials, the conductive additive on the metallic current collector. Electrons can be flowed in the electrode through electrical contacts of the active material-conductive additive-current. If the binder cannot effectively bind the components during charge and discharge cycling, ohmic resistance of the electrode increased and lowered performances are resulted. In the process of the electrode, in addition, the binder effects the slurry properties, which results in the electrode morphology, distribution of the active material particles and the conductive carbon particles.

Polyvinylidene fluoride (PVDF) is the most commercially used binder for lithium-ion batteries. This is due to its highest electrochemical stability from reductive potential (~ 0 V *vs*. Li/Li^+) to oxidative potential (~ 5 V vs. Li/Li^+), which can be confirmed from a calculation of lowest unoccupied molecular orbital (LUMO) and highest occupied molecular orbital (HOMO).[57] Based on this feature, PVDF has been used for graphite negative electrode and $LiCoO_2$ positive electrode. Nevertheless, PVDF requires to be dissolved in toxic and expensive organic solvent such as NMP.

Alternative water-soluble binders for graphite such as carboxymethyl cellulose (CMC) and styrene-butadien rubber (SBR) have been proposed.[58] Water is environmental friendly solvent and is important for large-scale electrode production. Water-soluble polymers having hydrophilic functional groups have been attracted much attention from a consideration of using high capacity negative electrode materials such as alloying material, Si or Sn. Among the water-soluble binders, CMC has been spotlighted, which is used for graphite negative electrode

earlier.[59,60] With using CMC as a binder for Si negative electrode, it has been understood that some features of it such as brittleness[61] and carboxylic acid groups having hydrogen bonding with surface hydroxyl groups or silanol group of Si surface[62-64] guarantees a good cycle performance. Another polymers such as poly(acrylic acid)[65-67], alginic acid[68] or nature-originated polymers[69-71] give also stable cycle performance in Si-based electrodes. CMC and PAA have been applied to the positive electrode material such as $LiCoO_2$[72], $LiFePO_4$[73-75], $LiNi_{0.5}Mn_{1.5}O_4$[76] and so on (Figure 3). However, application of these water-soluble binders to the positive electrode materials still have problems to be overcome, which includes instability of the positive active materials, slurry formulation, etc.[77]

Another class of the polymer binder is the conductive polymers. Although typical conductive polymers such as polyaniline, polypyrrole, and polythiophene have high electronic conductivity, utilization of them to use for binders is limited due to their low processing properties, they are cannot be dissolved in common solvents. Some researches about active material/conductive polymer composite by *in-situ* polymerization or mechanical methods have been tried.[78,79] Electronic conductive polymer such as poly(3,4-ethylene dioxythiophene)/poly(styrene-4-sulfonate) (PEDOT:PSS) have been utilized as binders.[80,81] PEDOT:PSS can be used for the electrode formulation because its particles are dispersed in an aqueous medium. Recently, a n-type conductive polymer based on fluorene for Si negative electrodes was developed, which can be formulated by the conventional electrode process.[82]

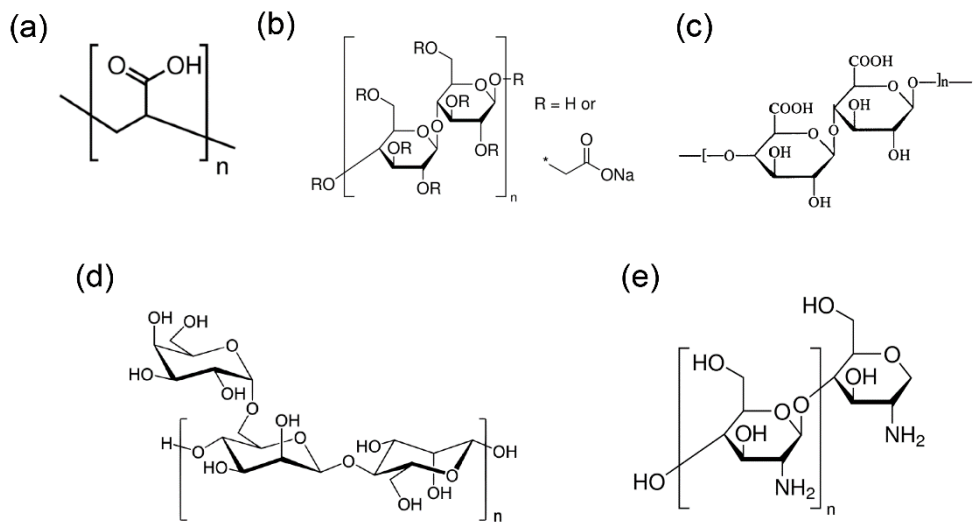

Figure 3. Some alternative binders: (a) poly(acrylic acid), (b) carboxymethyl cellulose sodium salt, (c) alginic acid, (d) guar gum, and (e) chitosan.

2. Electronic conductive polymer binder for Si negative electrode

2.1 Poly(phenanthrenequinone) as a conductivie binder for nano-sized silicon negative electrodes

2.1.1 Motivation and objectives

Over the last decades, graphite has been the most popularly used negative electrode since this crystalline carbon largely meets the requirements imposed on the negative electrodes of lithium-ion batteries (LIBs).[12,40,83] The market of LIBs is now expanding to electric vehicles (EVs) and energy storage systems (ESSs). However, because of the limited specific capacity for graphite, the alternatives having higher specific capacity have been highly sought. Si (theoretical capacity = 3579 mA h g_{Si}^{-1}) has emerged as a viable candidate.[84-87] The practical use of Si is, however, still hindered because of a critical problem that is associated with massive volume change upon cycling. The volume change frequently leads to a formation of cracks or pulverization of Si particles, which eventually causes a breakdown of electrically conductive network made between Si particles, conductive carbon particles and metallic current collector. To solve or at least mitigate this volume-change problem, many efforts have been made including the nano-structuring of Si[46-48,88] and introduction of a buffer matrix.[50-56,89] The nano-sizing approach seems promising

because the absolute volume change can be reduced.[90] However, another issue has emerged in this approach, which is the excessive loading of conductive carbon and polymeric binder. Namely, a large amount of conductive carbon is needed to make electric contacts with nano-sized Si particles because the surface area of nano-Si is much larger than that for the bulk-sized ones. Moreover, the use of an excessive amount of polymeric binder is inevitable in binding such a large number of Si and carbon particles. The loading of a large amount of inactive components (conductive carbon and polymeric binder) results in a decrease in the energy density of LIBs.

This work was motivated by a simple premise that the electrically conductive network can be made without conductive carbon if the polymeric binder itself is electrically conductive. That is, if this is possible, the conductive polymer by itself serves as both the conductive carbon and polymeric binder to minimize the loading of inactive components in the electrode layer. To implement this premise, the following points should further be considered. First, the candidate polymer should be electronically conductive within the working potential of Si (0.0–0.5 V vs. Li/Li^+) to serve as the electron transfer channel between the Si particles and the current collector. Second, the polymer should be uniformly dispersed with a strong binding ability within the electrode layer. Third, the loading of conductive polymer binder should be minimized to maximize the energy density of the cells. The p-type conducting polymers such as polyaniline and polypyrrole are discarded in this work because they are electronically conductive only at >3.0 V (vs. Li/Li^+).[91]

As the first part of chapter 1, a polymer derived from 9,10-phenanthrenequione (PQ) was synthesized and tested to determine whether it satisfies the above-mentioned requirements. The selection of PQ was based on its unique molecular structure. Namely, the conductive polymers to be employed as the binder for Si negative electrodes should have a very low value in the lowest

unoccupied molecular orbital (LUMO), such that they are readily reduced by n-doping to be electronically conductive in the working potential of Si. PQ seems to be one of the right choices because it is highly conjugated and has the electron-withdrawing carbonyl group.[82] Furthermore, the n-doping by two electrons/Li^+ ions per formula unit is possible due to the presence of two carbonyl substituents. One can assume a higher electronic conductivity than the reported conjugated polymer based on fluorenone on the basis of the n-doping (electron injection) at the polymers described in Figure 4. Through the n-doping more conjugated structure is formed in PPQ in which electrons can be moved faster.

To assess the binder performance of PPQ, a composite electrode was prepared from a mixture of nano-sized Si powder and the conducting polymer (PPQ) without conductive carbon, and its electrode performances were examined. For comparison purposes, another composite electrode was prepared with poly(acrylic acid) lithium salt (LiPAA), which is a non-conductive binder.

2.1.2 Experimental

2.1.2.1 General procedure for the synthesis of the conductive polymer binder

Sample powder of 3,6-Poly(phenanthrenequinone) (PPQ) was provided by Prof. Young Gyu Kim's group at Seoul National University. The polymer was synthesized by using the Suzuki coupling reaction, which is presented in a previous report.[92] In detail, a solution of 3,6-dibromophenanthrene-9,10-dione (compound **1** in Figure 5) (0.50 g, 1.52 mmol) and 3,6-bis(4,4,5,5,-tetramethyl-1,3,2-dioxaborolan-2-yl)phenanthrene-9,10-dione (compound **2** in Figure 4) (0.70 g, 1.52 mmol) in toluene (80 mL) and THF (20 ml) was stirred in round flask. Then, $Pd(PPh_3)_4$ (15.6 mg, 0.15 mmol), Na_2CO_3 (2 ml, 2.0 *M* in distilled water) and Aliquat 336 (1 ml) as a phase transfer catalyst were added. The reaction mixture was stirred vigorously for 2 days at 110 °C, and the resulting crude mixture was concentrated by rotary evaporator and precipitated in methanol/H_2O/1.0 *N* HCl mixture (ratio of 10/10/1 v/v).[82,93,94] The precipitate was centrifuged and dried in air. The dried polymer (compound **3** in Figure 4) was fractionated by soxhlet extraction with methanol and dichloromethane. Residue deep brownish solid was collected and dried under vacuum. GPC (DMF, PMMA standard): Mn = 5900, Mw = 6138, Mw/Mn = 1.04.

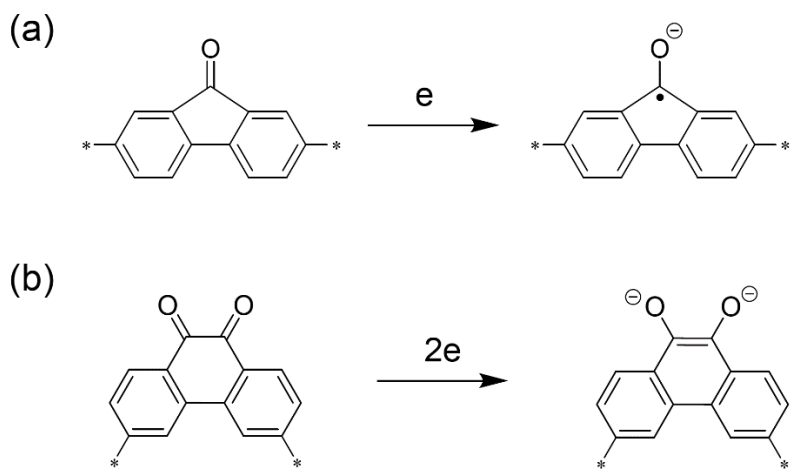

Figure 4. Proposed formation of radical anions (n-doping) in (a) poly(fluorenone) and (b) poly(phenanthrenequinone).

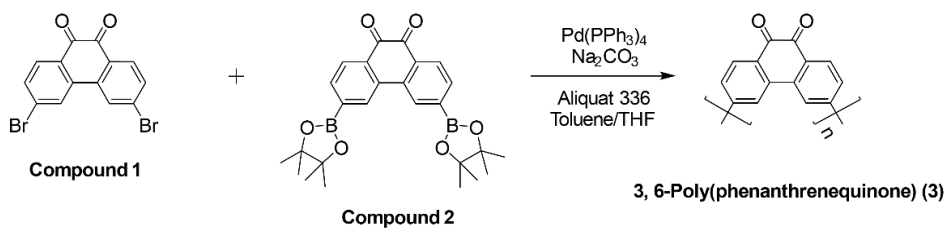

Figure 5. Synthetic procedure of poly(phenanthrenequinone).

2.1.2.2 Electrode preparation

To examine the electrochemical performances of PPQ itself, a composite PPQ electrode was fabricated. To this end, PPQ was dissolved in *N*-methyl-2-pyrrolidone (NMP, anhydrous, 99.5 %), and the resulting viscous solution was dispersed on a piece of Cu foil (current collector) and dried at 120 °C. The PPQ is deposited as a film on Cu foil.

Two different nano-Si composite electrodes were prepared by using either PPQ or LiPAA as the binder. For the nano-Si/PPQ composite electrode, PPQ was dissolved into NMP, into which nano-sized Si powder (crystalline, APS ≤ 50 nm, 98 %, laser synthesized from vapor phase, Alfa Aesar, Figure 6) was dispersed. The resulting slurry was coated on a piece of Cu foil and dried at 120 °C. The PPQ loading was varied at 10–30 wt. %. For the nano-Si/LiPAA composite electrode, poly(acrylic acid) (PAA, average Mv ~ 450000) and lithium hydroxide (LiOH, ACS reagent, ≥ 98.0 %) were dissolved into de-ionized water, into which the nano-Si powder was dispersed. The resulting slurry was coated on a piece of Cu foil and dried at 120 °C. The LiPAA loading was 30 wt. %. Si loading in the composite electrodes was 0.46 mg cm^{-2} for Si-LiPAA (7:3), 0.55 mg cm^{-2} for Si-PPQ (7:3) and 0.70 mg cm^{-2} for Si-PPQ (9:1), respectively. Electrode thickness was 9 μm for Si-LiPAA (7:3), 12 μm for Si-PPQ (7:3) and Si-PPQ (9:1), respectively. Electrode porosity was 65 % for Si-LiPAA, 69 % for Si-PPQ (7:3) and 70 % for Si-PPQ (9:1), respectively.

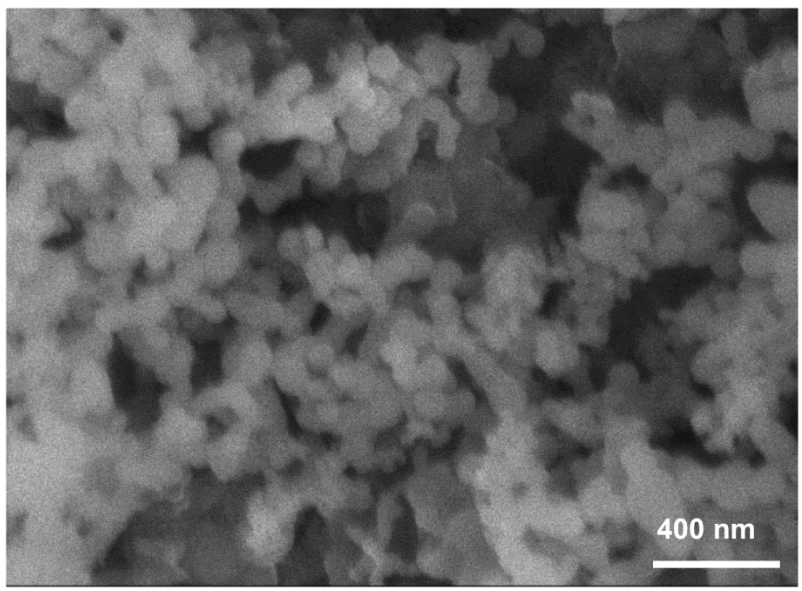

Figure 6. FE-SEM image of nano-sized Si powder.

2.1.2.3 Cell preparation

To examine the electrochemical performances of PPQ itself, a Li/PPQ cell (2032 coin-type, electrode diameter = 11 mm) was fabricated with lithium foil (as a counter and reference electrode), and polypropylene (PP)/polyethylene (PE)/PP tri-layer separator. The used electrolyte was 1.0 M $LiPF_6$ dissolved in ethylene carbonate (EC)/diethyl carbonate (DEC) (1:1, vol. ratio). Li/nano-Si cells (2032 coin-type) were also fabricated to characterize the electrode performance of nano-sized Si electrodes. To this end, the nano-Si/PPQ and nano-Si/LiPAA composite electrodes were loaded into the coin cells along with Li foil. The used electrolyte was 1.3 *M* $LiPF_6$ dissolved in EC/fluoroethylene carbonate (FEC)/DEC (2:2:6, vol. ratio). The PP/PE/PP tri-layer separator was used.

2.1.2.4 Electrochemical characterizations

2.1.2.4.1 Charge-discharge test

The galvanostatic lithiation (charge) and de-lithiation (discharge) cycling of Li/PPQ and Li/nano-Si cells were conducted using a TOSCAT-3100 (TOYO SYMSTEM CO., LTD.) at 25 °C in a constant current-constant voltage (CC-CV) mode. In the case of Li/PPQ cell, the galvanostatic charge-discharge cycling was performed at a current density of 50 mA g_{PPQ}^{-1} at in the voltage range of 0.005~3.0 V (vs. Li/Li^+). In the case of Li/nano-Si cells, pre-cycling step was added in order to obtain full

activation of Si active material and generation of stable solid electrolyte interphase (SEI) layers on the Si particles. To this end, the galvanostatic charge-discharge cycling was performed 2 cycles. The current density was 100 mA g_{Si}^{-1} for the first cycle and increased to 200 mA g_{Si}^{-1} for the second cycle. The voltage range was 0.005–1 V. For the cycle performance characterization of Li/nano-Si cells, the current density was fixed at 358 mA g_{Si}^{-1} (0.1 C- rate). The cycle number is counted from the following lithiation/de-lithiation. For the rate capability test, the de-lithiation current was varied from 0.1 C to 3 C after the pre-cycling while the lithiation current being fixed at 0.1 C.

2.1.2.4.2 Galvanostatic intermittent titration technique (GITT)

Galvanostatic intermittent titration technique (GITT) was employed to monitor the evolution of internal resistance upon cycling in the Li/nano-Si cells. To this end, a series of current pulse (0.1 C for 10 min) and rest (for 30 min) was applied over the potential range of 0.005~1.0 V. In each rest period, the cell voltage was traced by using a battery cycler (WBCS3000) at 25 °C (Figure 7). The voltage value right after the current pulse and at the end of rest was taken in each current pulse as a closed-circuit voltage (CCV) and quasi-open-circuit voltage (QOCV), respectively, from which the cell polarization is calculated as the difference between the end of CCV and QOCV. The internal resistance of the cells was then calculated by the following relationship:[95] Internal resistance (Ω g) = Cell polarization (V) / Applied current (A g^{-1}).

2.1.2.4.3 Electrochemical impedance spectroscopy (EIS)

To examine the conductive nature of the PPQ film electrode as a mixed conductor or an active material according to its state of charge and to identify the resistance of the Li/nano-Si cells, AC impedance of the cells were measured using IM6e (Zahner) electrochemical station. Measurements were performed with frequency range of 100 kHz–10 mHz and a 5 mV amplitude. In the case of the Li/PPQ cell, measurements were conducted with various state of charge: at open-circuit voltage (OCV), first lithiated to 5 mV, de-lithiated to 3 V and second lithiated to 5 mV. In the case of the Li/nano-Si cells, pre-cycling of the cells was conducted prior to EIS measurements. The cells were left to show OCV of 0.5 V after 1 cycle.

2.1.2.5 Morphology characterizations

Particle morphology and size of nano-Si powders were examined using field emission scanning electron microscopy (FE-SEM, JEOL JSM-6700F). To observe the morphology of the nano-Si composite electrode with LiPAA and PPQ binder, transmission electron microscopy (TEM) was used. TEM measurement was performed using JEM-ARM200F (JEOL, Japan) operated at 200 kV. In order to identify the polymer from the composite, imaging with bright-field scanning TEM (BF-STEM) and elemental mapping with energy dispersive x-ray spectroscopy (EDS) were performed. Samples were prepared by dropping dispersion of the nano-Si/polymer binder composite onto a lacey carbon-coated Cu grid and drying overnight under vacuum.

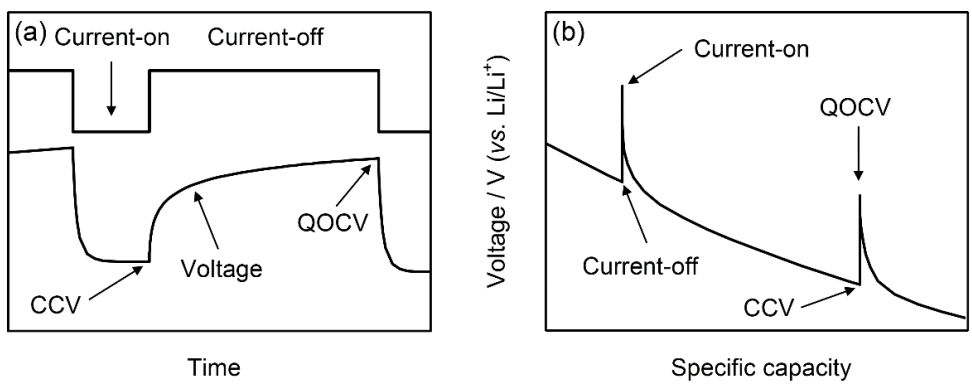

Figure 7. Galvanostatic intermittent titration technique (GITT). (a) Current input and the corresponding voltage behavior, (b) voltage transient according to the capacity.

2.1.3 Results and discussion

Galvanostatic charge-discharge voltage profiles of the Li/nano-Si cell fabricated with two different polymer binders are shown in Figure 8 and the corresponding differential capacity (dQ/dV) plots are provided in Figure 9. In both electrodes with the two binders, a long plateau at the first lithiation corresponds to the formation of amorphous Li_xSi (two-phase reaction). Because the lithation is allowed to 5 mV, crystalline $Li_{15}Si_4$ is expected to be formed and this is confirmed by another plateau (0.44 V) at the subsequent de-lithiation. Two plateaus at the second lithiation correspond to the lithiation of amorphous Si (single-phase reaction).[84] Characteristic peak of formation of crystalline $Li_{15}Si_4$ reported elsewhere is not observed in our experiment. This might be due to polarization. The first de-lithiation capacity delivered by the nano-Si electrode with the LiPAA binder is much smaller (2471 mA h g_{Si}^{-1}) than the theoretical value (3579 mA h g_{Si}^{-1}) even if the charge/discharge rate is very slow (0.028 C), illustrating that all the nano-Si particles are not utilized for lithiation/de-lithiation. Such an incomplete utilization is ascertained with a control experiment, in which carbon black (Super P) is added into this electrode as a conductive agent and cycled in the same condition. As seen in Figure 10, the de-lithiation capacity now increases up to 2883 mA h g_{Si}^{-1}, showing that the utilization of nano-Si particles increases due to the reinforcement of the electrically conductive network by the presence of carbon black, which is illustrated in Figure 11. When LiPAA is replaced by the PPQ binder, however, the nano-Si electrode delivers a de-lithiation capacity of 3271 mA h g_{Si}^{-1} at the same rate (0.028 C), which is 91 % of the theoretical value. This feature ensures that continuous current paths are made in the latter electrode even without carbon black due to the

electrically conducting role of PPQ binder.[96]

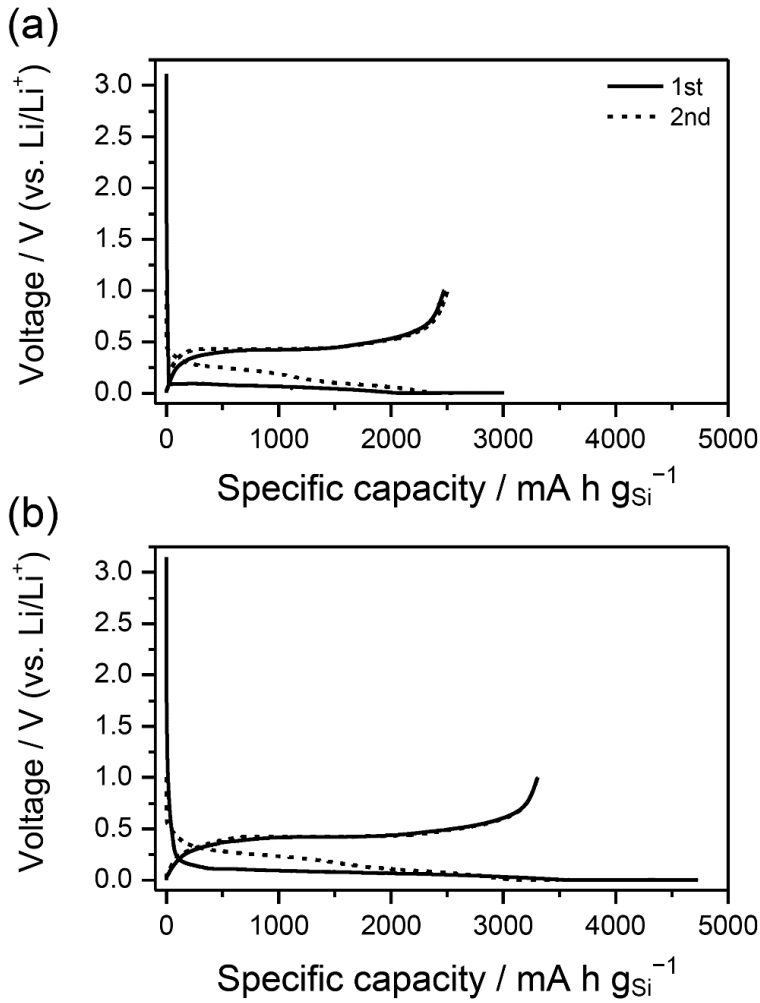

Figure 8. The charge-discharge voltage profiles of Li/nano-Si cells fabricated with LiPAA binder (a) and PPQ binder (b) in the initial two cycles (pre-cycling period).

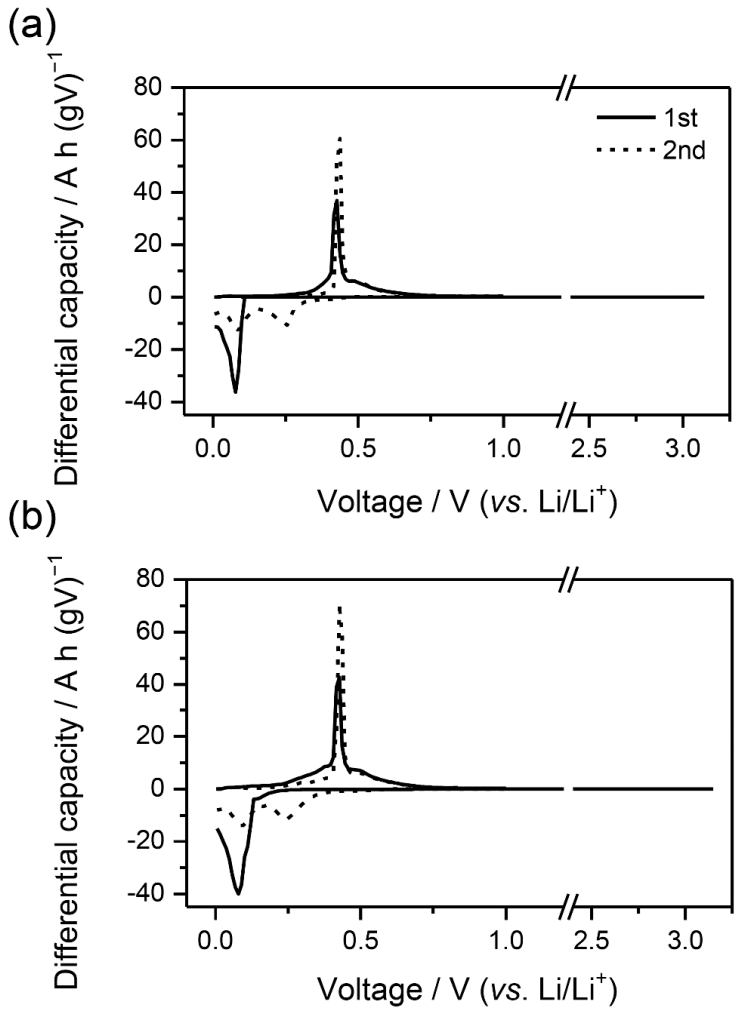

Figure 9. The corresponding differential capacity (dQ/dV) plots of Figure 8.

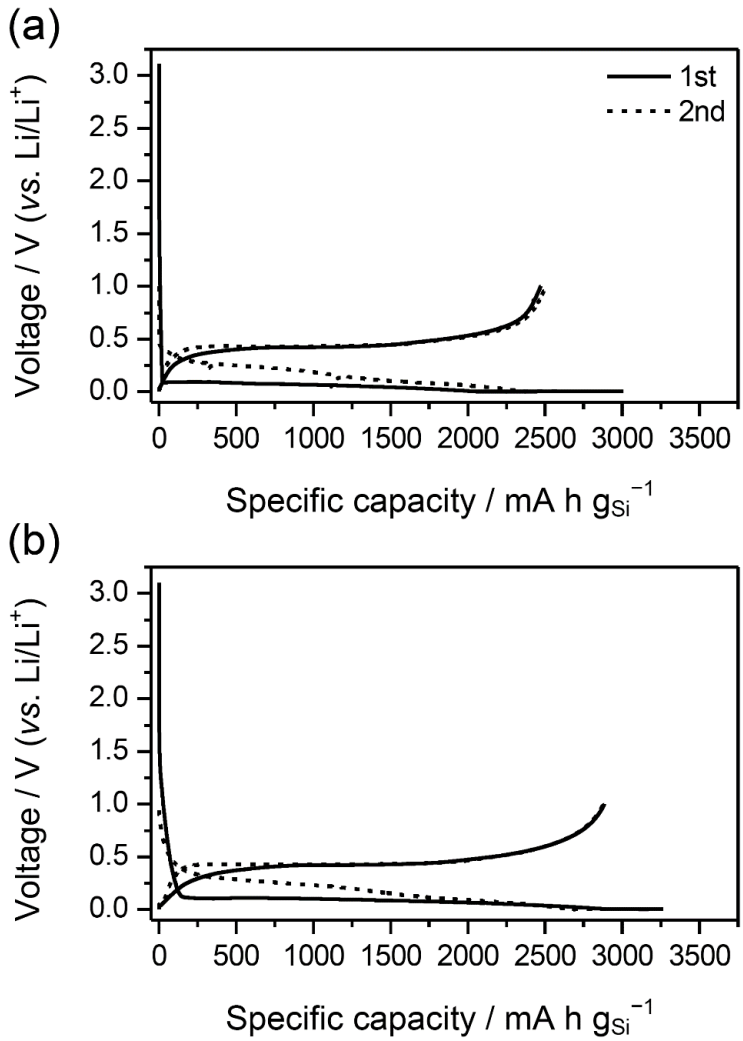

Figure 10. The charge-discharge voltage profiles of Li/nano-Si cells fabricated with LiPAA binders. (a) The composite electrodes were prepared without (a) and with (b) conductive carbon (super P). In the case of the electrode with super P, the electrode was comprised of nano-Si powder, conductive carbon, and LiPAA (5:2:3, weight ratio).

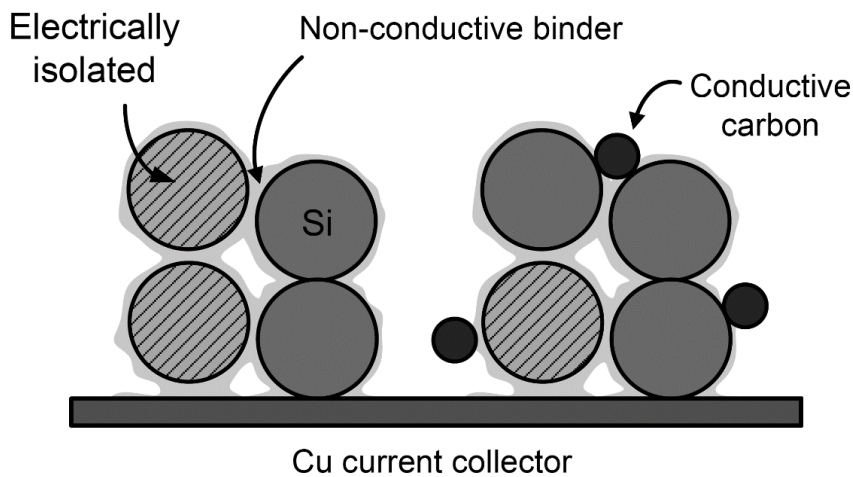

Figure 11. Schematic representation of the nano-Si electrode fabricated without and with the conductive carbon.

To confirm the conducting role of PPQ, the PPQ by itself is deposited on Cu foil as a film and the resulting Li/PPQ cell is charge/discharge cycled (Figure 12a). In this cell, the PPQ film is lithiated up to 1239 mA h g_{PPQ}^{-1} in the first cycle but de-lithiated to 372 mA h g_{PPQ}^{-1}. The large lithiation capacity at about 0.15 V in the first cycle shows that the PPQ film takes electric charges of 1239 mA h g_{PPQ}^{-1} and the equivalent amount of Li^+ ions. That is, the PPQ film is n-doped by taking electrons and Li^+ ions in this potential region: the PPQ film becomes mixed-conducting like the electrode materials used in lithium-ion batteries. This is also confirmed by that impedance of the PPQ film electrode increased with decreased amount of charge (de-lithiated state) and decreased with increased amount of charge (lithiated state), as which is shown Figure 12b. By the way, the much smaller first de-lithiation capacity implies that large amount of electrons/Li^+ ions are trapped inside the PPQ matrix. This trapping is undesirable in one sense because it causes an irreversible capacity when used as the binder. Hence, the PPQ loading should be minimized. However, the Li trapping is beneficial in the other sense because PPQ maintains its mixed-conducting property once it is lithiated in the first cycle.

The n-doping for the PPQ binder that is formulated with the nano-Si powder is confirmed in Figure 13, in which the first differential lithiation capacity plot of the Li/nano-Si cell (with PPQ binder, Figure 9) is magnified. A shoulder (0.1~0.15 V) overlaps the lithiation peak of Si. The shoulder must be responsible for the lithiation of PPQ binder because it does not appear with LiPAA binder. In addition, the position of shoulder is very close to the lithiation peak for the pure PPQ film electrode (0.15~0.18 V). The slight shift to the negative potential (polarization) must be due to the presence of less conductive Si particles in the nano-Si/PPQ composite electrode. In short, the PPQ binder in the composite electrode becomes electrically conductive by n-doping in the first cycle and plays the conducting role thereafter. As

reversible capacity of Li/nano-Si cell fabricated additional conductive additive is increased more nano-Si particles take part in the electrochemical charge and discharge reaction thanks to PPQ conductive binder. In Table 2, de-lithiation capacity by PPQ itself in the composite electrode and by nano-Si are compared with de-lithiation capacity in the Li/nano-Si cell fabricated with LiPAA binder. In the de-lithation capacity of Li/nano-Si cell at the first cycle, 2313 mA h g_{Total}^{-1}, the capacity from PPQ itself is only 38 mA h g_{Total}^{-1} and the capacity from the nano-Si is 2275 mA h g_{Total}^{-1} which is 546 mA h g_{Total}^{-1} larger than the capacity of the Li/nano-Si cell fabricated with LiPAA binder.

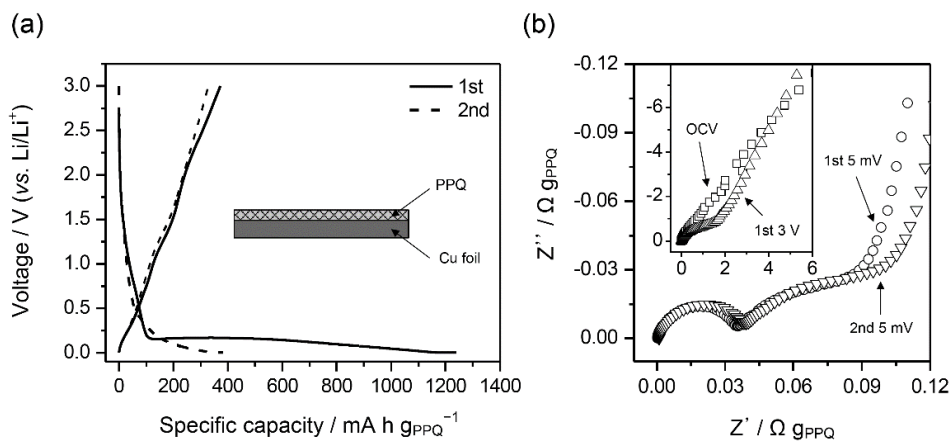

Figure 12. (a) The charge-discharge voltage profiles of the Li/PPQ cell in the initial two cycles. (b) AC impedance results of the Li/PPQ cell, which is measured at OCV, after first lithiation and de-lithiation, and second lithiation.

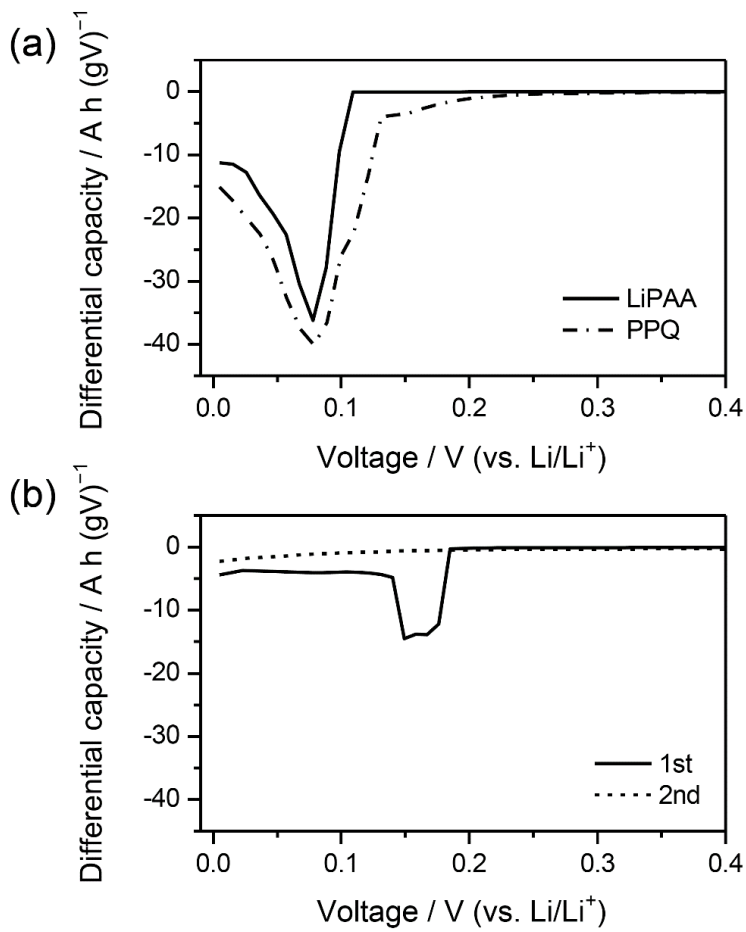

Figure 13. The magnified view of the first differential capacity plots in the lithiation period of Li/nano-Si cells and Li/PPQ cell.

Table 2. De-lithiation capacity of Li/nano-Si cells based on the total electrode weight (mA h g_{Total}^{-1}). De-lithiation capacity of PPQ itself is calculated when de-lithiation voltage cut-off is 1 V at the first cycle in Figure 12a: 125 mA h g_{PPQ}^{-1}.

	Si-PPQ	Si-LiPAA
PPQ	38	-
Si	2275	1729
Total	2313	1729

To highlight the conducting role of the PPQ binder, a rate test is performed with two nano-Si composite electrodes fabricated with two binders. The electrode fabricated with the PPQ binder outperforms the other one with respect to rate property (Figure 14). The de-lithiation capacity difference of two electrodes is not big at a slower rate (0.1 C), but becomes larger with an increase in the de-lithiation current. At 3 C (ca. 10 A g_{Si}^{-1}), the nano-Si electrode with PPQ binder delivers a de-lithiation capacity up to 2362 mA h g_{Si}^{-1}, contrasted by the electrode prepared with LiPAA which delivers 439 mA h g_{Si}^{-1} at the same rate. This means that the electrically conductive network is well-made with the PPQ binder, which is not the case with the LiPAA binder. The Li/nano-Si cell fabricated with LiPAA binder shows larger polarization at high de-lithation current, so Li^+ and electron cannot be extracted from the electrode because voltage arrives cut-off voltage quickly. This is not the case in the Li/nano-Si cell fabricated with PPQ binder (Figure 15). The internal resistance of two electrodes is compared to show the differences in the conducting role of two binders. The Li/nano-Si cell with LiPAA shows a decrease in the internal resistance from 0.3 V in the lithiation period (Fig. 16b), which is due to a decrease in contact resistance at the particle-to-particle and/or particle-to-current collector contacts, caused by the volume expansion of the Si particles.[95] and increase of electrical conductivity because of formation of conductive Li-Si alloy. Slight increase of internal resistance in lower voltage (below 0.15 V) is due to the formation of less conductive Li-Si alloy.[97] In the de-lithiation period, the internal resistance rapidly increases from 0.4 V due to contact loss caused by volume contraction of Si particles. The evolution of internal resistance with PPQ binder is, however, quite different to that observed with LiPAA. The internal resistance is already marginal before the major lithiation of Si takes place at ca. 0.3 V, from which the contact resistance is supposed to be reduced due to the expansion of Si particles.

This implies that the electrically conductive network is already well-made during the pre-cycling stage. Even in the voltage range in which the nano-Si particles are expanded by lithiation and direct contacts between nano-Si particles are increased, the internal resistance of the electrode with PPQ binder is lower (Figure 17). Although electrical conductivity of lithiated Si becomes higher, electrons cannot be transferred through LiPAA binder but can be through PPQ binder. In the forthcoming de-lithiation, the internal resistance increases from 0.4 V due to Si contraction but to a much lesser degree than that observed with LiPAA binder. A practical important feature here is that the internal resistance remains marginal at 0.0~0.5 V, within which the Si electrode is charged/discharged.

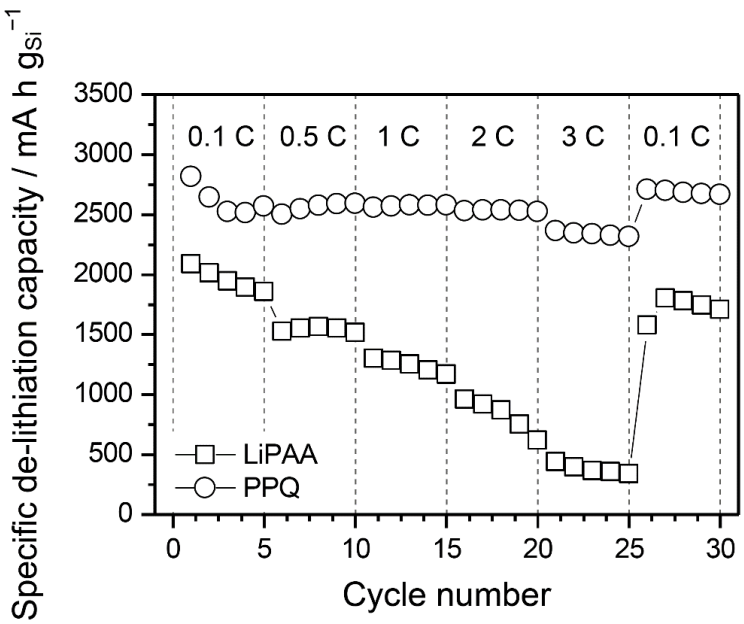

Figure 14. Rate capability of Li/nano-Si cells with two binders (30 wt.%). The de-lithiation current is indicated. For the lithiation, a constant current mode was used at 0.1 C.

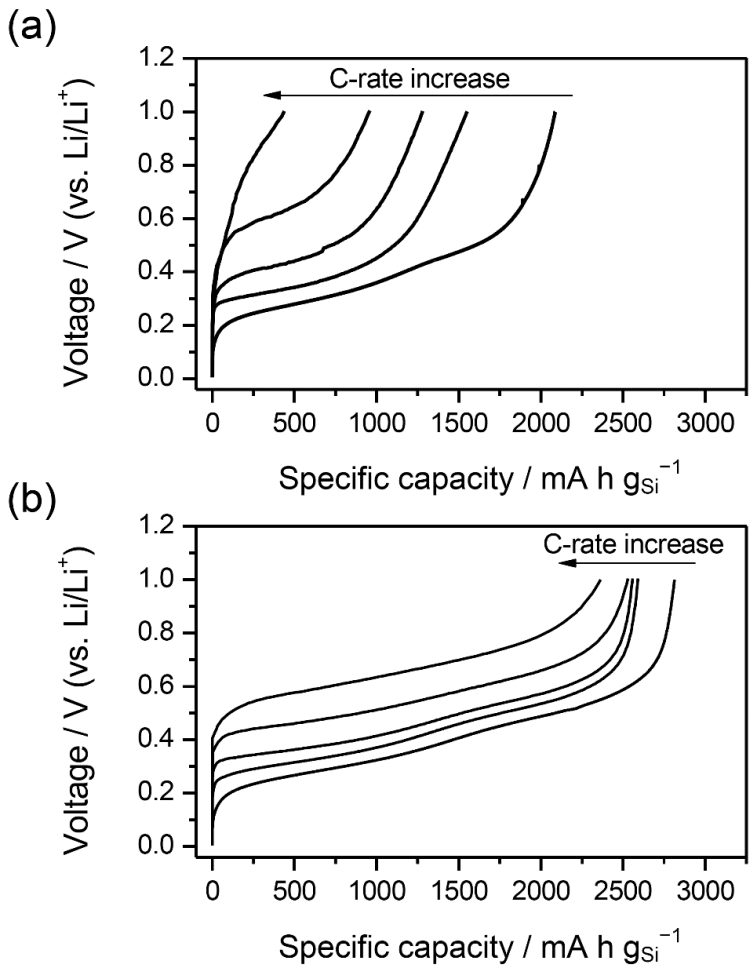

Figure 15. Discharge voltage profiles of Li/nano-Si cells fabricated with (a) LiPAA and (b) PPQ binder. The de-lithiation currents are 0.1, 0.5, 1, 2, and 3 C, respectively.

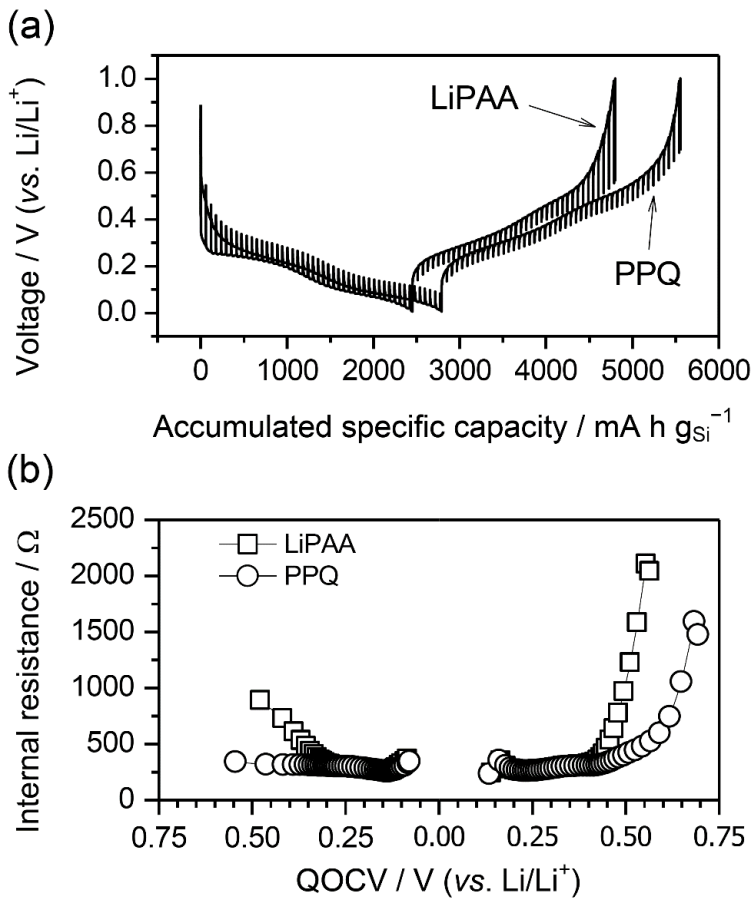

Figure 16. (a) The transient voltage profiles obtained from the galvanostatic intermittent titration technique (GITT) and (b) the evolution of internal resistance derived from the difference between the end of closed-circuit-voltage (CCV) and the quasi-open-circuit voltage (QOCV). The GITT experiment was carried out after two charge-discharge cycles (pre-cycling).

The difference in the internal resistance of the Si electrode with LiPAA and PPQ was greater in de-lithiation than lithiaion, especially above 0.4 V. For identification of which resistance mainly make this difference, ac impedance measurement was performed at 25 °C. Pre-cycled Si composite electrodes with two binders were further lithiated and de-lithiation was stopped before cell voltage reached 1 V. The cells were left to show OCV of 0.5 V. Ac impedance measurements were conducted with frequency range of 10 mHz ~ 100 kHz and amplitude of 5 mV. The result spectra and their fitting results are shown in figure 18. The elements shown in inset such as R_{Ω}, R_{SEI} and R_{ct} are the total ohmic resistance which includes the electrolyte and the electrode resistance, the resistance of solid electrolyte interphase (SEI), and charge transfer resistance, respectively. C_{SEI} and C_{dl} are constant phase element (CPE).[98] Note that the ESR and the R_{SEI} of the cells with the two electrodes did not show considerable difference. However, the charge transfer resistance (R_{ct}) of the cell with the electrode with LiPAA (1.047 Ω g) was larger seven times than that with PPQ (0.139 Ω g). This difference is originated from whether the binder can transfer electrons or not as discussed above.

As mentioned in the introduction, it is necessary for any conducting polymer binders to be uniformly dispersed within the electrode layer to effectively play a conducting role. Figure 19 shows the TEM images of two composite electrodes. The positions of Si and polymers can be identified from the elemental mapping of Si (Figure 19d and 19h) and carbon (Figure 19c and 19g). As is seen in the figure 19a~19d, the nano-Si particles are fully covered by the LiPAA layer, which is known as a surface-covering binder.[66,99] A similar full coverage of nano-Si by PPQ is observed in Figure 19e~19h. Such uniform coverage by the conductive PPQ layer offers effective current paths between the whole Si surface and the current collector allowing high utilization of Si particles and enabling high-rate

charge/discharge for this electrode. When the insulating LiPAA binder is used, however, the current paths are formed only through the Si particle-to-particle contacts; therefore, the electrode resistance is large. This is described in a schematic representation (Figure 20).

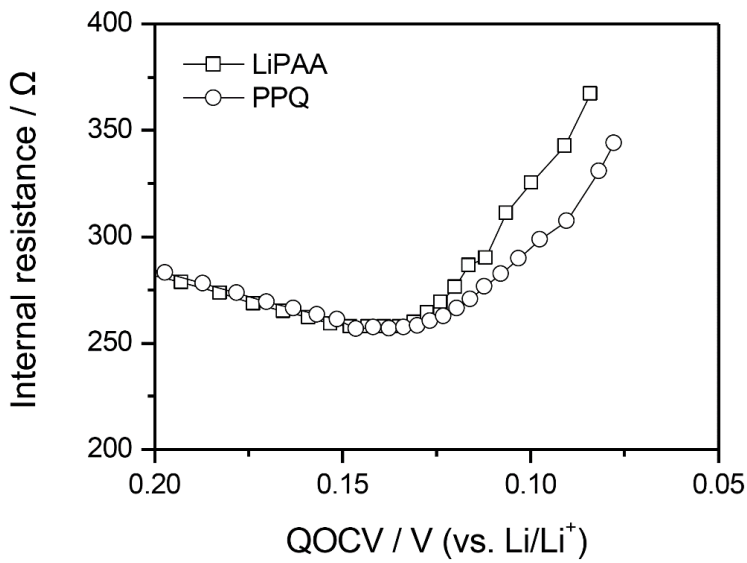

Figure 17. Evolution of internal resistance below 0.2 V QOCV during lithiation (magnified view of Figure 16b).

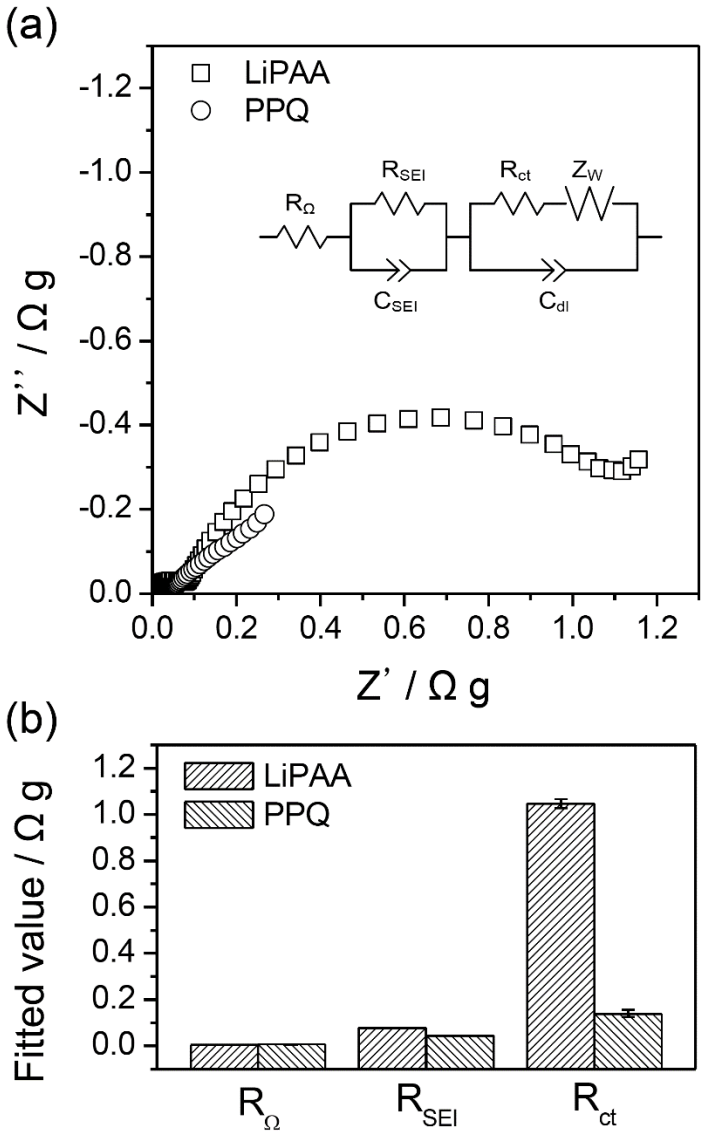

Figure 18. (a) AC impedance spectra of Li/nano-Si cells fabricated with two binders and (b) fitting results by inset equivalent circuit. The The measurements were made at 0.5 V after third lithiation. Before the measurements, the cells were de-lithiated to 0.5 V and OCV of the cells allowed to maintain 0.5 V by constant-voltage de-lithiation.

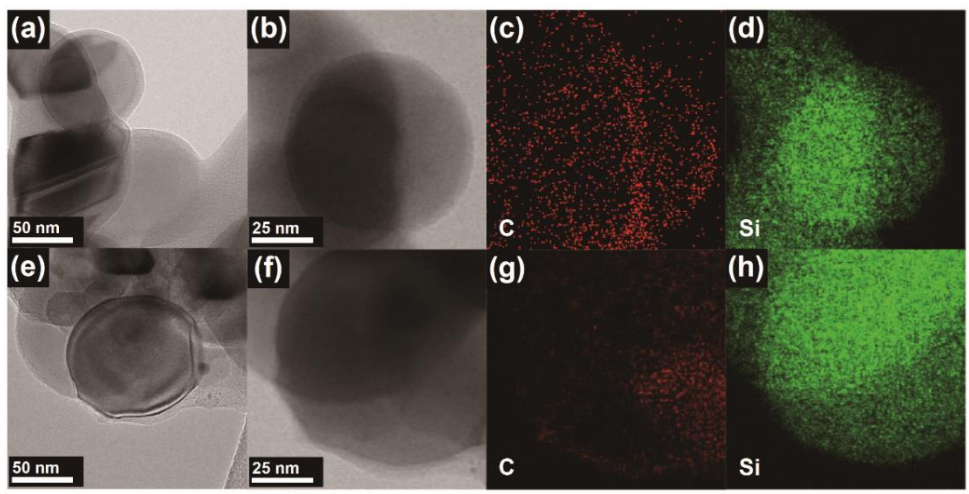

Figure 19. TEM images of the nano-Si/polymer binder composites: (a–d) LiPAA and (e–h) PPQ. The bright-field STEM images and their EDS maps: (b–d) LiPAA and (f–h) PPQ. The red and green dots represent C and Si, respectively.

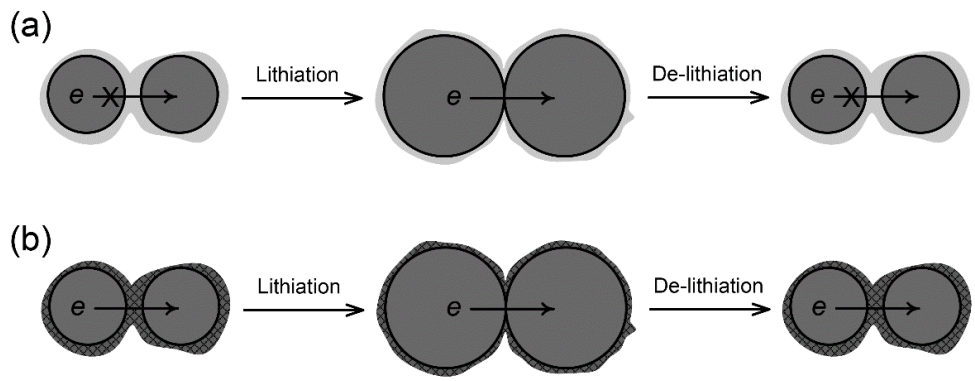

Figure 20. Schematic representation of electron conduction between the nano-Si particles covered with (a) LiPAA and (b) PPQ binder during lithiation and de-lithiation.

Figure 21 presents the cycle performance of two Li/nano-Si cells. The nano-Si electrode fabricated with 30 wt. % of PPQ shows a de-lithiation capacity of 3258 mA h g_{Si}^{-1} in the first cycle and 2823 mA h g_{Si}^{-1} in the 50th cycle, which is larger than those for the electrode fabricated with 30 wt. % of LiPAA. The larger capacity of the former electrode must be because of the almost full utilization of the Si particles due to the well-developed current paths. The reasonably good cycle retention explains the electrochemically stable nature of the PPQ binder. A binder content of 30 wt. % is far from practical because of its massive volume occupation by light-weight polymers. In the case of PPQ binder, the minimization of binder loading is even more important because PPQ causes an irreversible capacity (Figure 12). Along this line, the PPQ loading is decreased to 10 wt. %, which is close to that used for practical electrode formulations. As is seen in Figure 21a, de-lithation capacity of the electrode with 10 wt. % PPQ loading is lower than the electrode with 30 wt. % loading. This trend is inversed when the capacity is calculated based on the total electrode weight (Figure 21b). Because the amount of the PPQ binder is lower, in other words, the amount of active material, nano-Si, is higher, de-lithiation capacity of the electrode with 10 wt. % PPQ loading is higher. This implies that high energy density of the nano-Si electrode can be achieved by lowering the amount of PPQ loading. The evolution of Coulombic efficiency for three Si composite electrodes is presented in Figure 22. All the Si electrodes show a Coulombic efficiency of less than 97 % in the pre-cycling stage (initial two cycles), but the values are retained at >97 % thereafter. In the case of the nano-Si electrode fabricated with 30 wt. % of PPQ (Si:PPQ = 7:3), the Coulombic efficiency is as low as 70 % in the first cycle during the pre-cycling step due to large irreversible capacity. Two origins can be assumed for the irreversible capacity. One is the uptake of Li^+ ions/electrons by the PPQ binder in the first lithiation period (Figure 12) and the

other is the consumption of Li^+ ions/electrons for the reductive electrolyte decomposition on the Si electrode surface. Note that the used Si is nano-sized (surface area = 57 $m^2\ g^{-1}$), such that the second contribution seems to be appreciable. This feature is ensured by the observation that the first Coulombic efficiency is 82 % for Si:LiPAA = 7:3, in which only the electrolyte decomposition prevails since Li trapping is absent for LiPAA binder. Meanwhile, the Si:PPQ = 9:1 composite electrode, in which the PPQ loading was reduced to mitigate the contribution from the Li trapping by PPQ binder, gives a Coulombic efficiency of 77 % in the first pre-cycle, which is comparable to that observed with Si:LiPAA = 7:3 (82 %). Presumably, the irreversible capacity that is associated with the electrolyte decomposition is dominant over that coming from Li trapping in the Si:PPQ = 9:1 composite electrode. A simple calculation, which was performed on the basis of Li trapping by PPQ (Figure 12) and the theoretical capacity of Si (3579 mA h g_{Si}^{-1}), shows that the Li trapping by PPQ binder in Si:PPQ = 9:1 electrode is 87 mA h g_{Total}^{-1}, which is marginal as compared to the capacity delivered by the Si component (3221 mA h g_{Total}^{-1}). Here, the subscript "Total" means the sum of the weight of Si and PPQ binder. This feature manifests itself that the irreversible capacity caused by Li trapping can be reduced by decreasing the PPQ loading in the composite electrode as far as the electrode performance is not seriously deteriorated.

Another way to prevent the irreversible capacity caused by Li trapping is the use of pre-lithiated PPQ binder. Namely, if PPQ can be lithiated by chemical or electrochemical methods, and the pre-lithiated PPQ is chemically stable at ambient conditions, it can be added as a binder through the conventional slurry preparation method. Unfortunately, the pre-lithiated PPQ by electrochemical reaction exhibits a poor solubility in the common organic solvents. Furthermore, the pre-lithiated PPQ loses the mixed conducting behavior once it is exposed to ambient conditions,

probably due to the reactions with moisture water and oxygen.

How electrons move in the nano-Si composite electrodes is illustrated in Figure 23 schematically. If the composite electrode is composed of active material and non-conducting polymer binder without conducting agent (control group in this work), electron conduction pathways are only formed by particle-to-particle or particle-to-current collector contacts (Figure 23a). The electronic conduction, namely, is limited to the direct contacts. Conventionally, to enhance the electrical conductivity of electrodes, particulate conducting agent such as carbon black is added (Figure 23b). However, limited contacts of the conducting agent make it difficult to connect electrically all particles and current collector. This may be solved by using of large amount of conducting agent. But, this cannot be a realistic alternative in the view point of energy density. On the other hand, the networks by the conducting polymer binder make it possible to transport electrons to everywhere in the electrode without the conventional particulate conducting agent (Figure 23c). In this point of view, development of conducting polymer binder like PPQ can be a shortcut to the commercialization of Si electrodes.

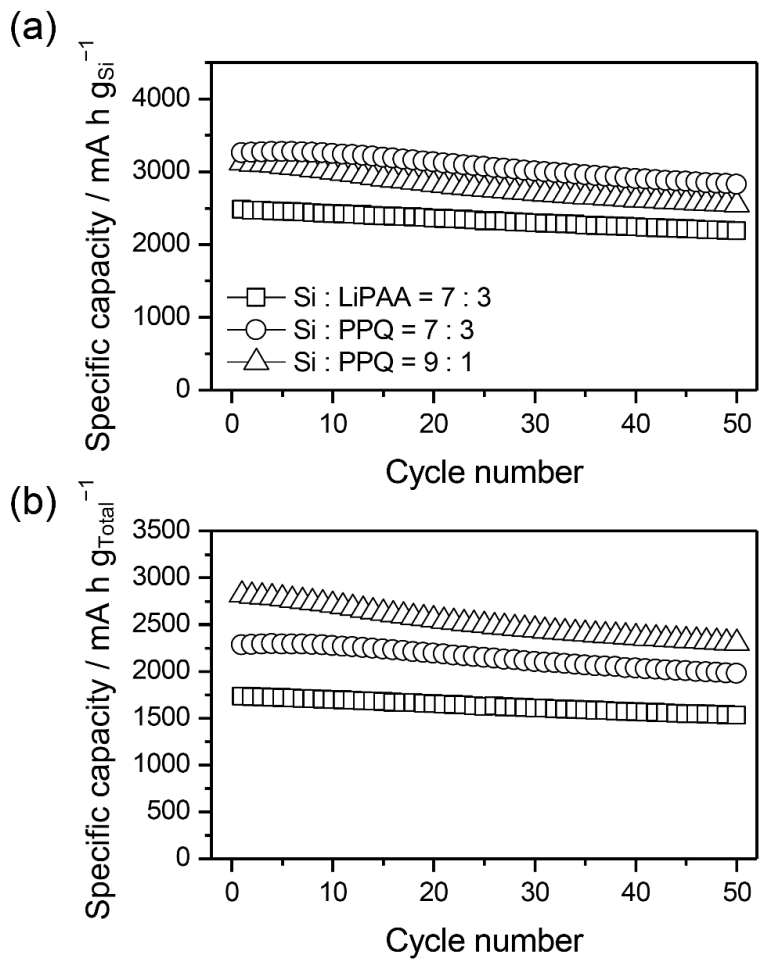

Figure 21. Cycle performance of Li/nano-Si cells (pre-cycling data are excluded). Specific capacity is calculated based on the weight of nano-Si, the active material (a) and total weight of the electrode (b). De-lithiation capacity is only displayed.

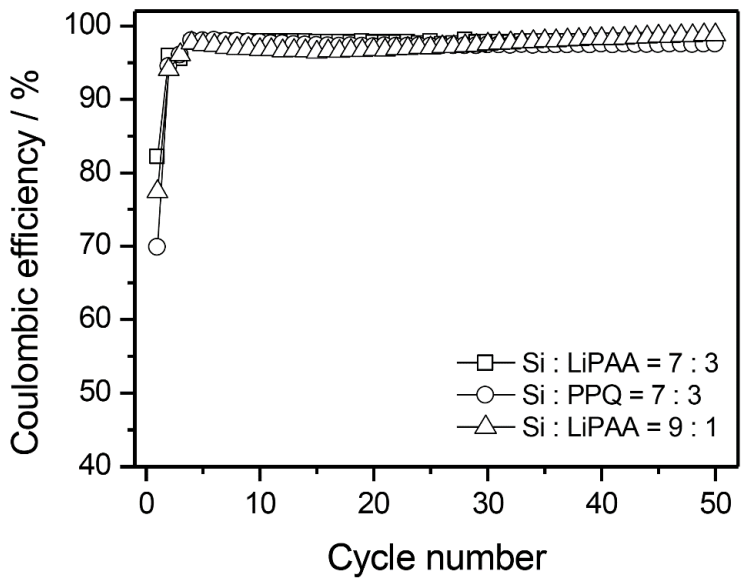

Figure 22. Coulombic efficiency of Li/nano-Si cells. Data at pre-cycling are included.

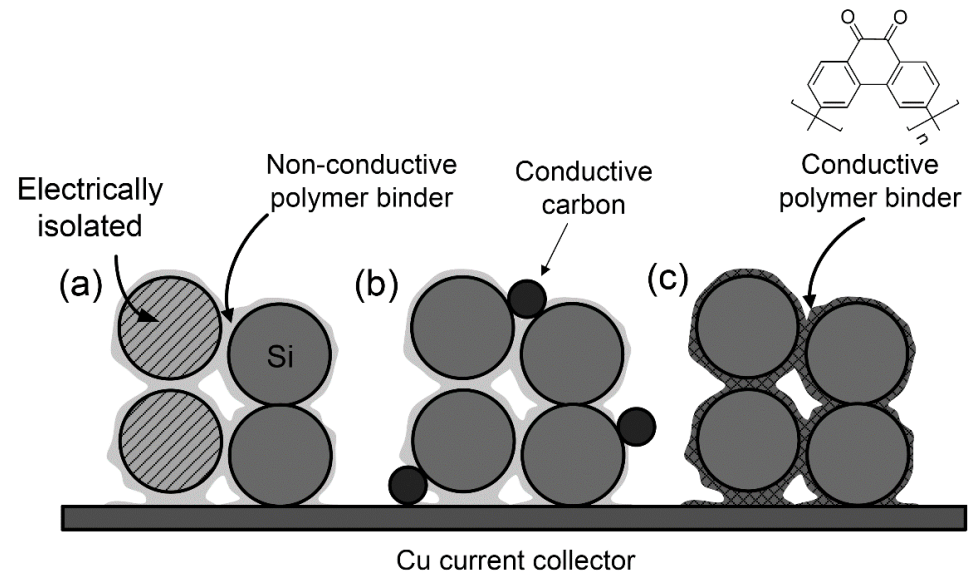

Figure 23. Electron conduction pathways in various nano-Si composite electrodes. (a) Without conducting agent: particle-to-particle or particle-to-current collector contacts. (b) With particulate conducting agent: enhanced electrical contacts but still remained disconnections. (c) Conducting binder: electrons can freely move within the electrode.

2.2 Poly(phenanthrenequinone)-poly(acrylic acid) composite as a conductive polymer binder for submicrometer-sized silicon negative electrodes

2.2.1 Motivation and objectives

Although nano-sized Si has advantages such as higher capacity due to the lowered volume change effect and superior cycle performance, it has still some problems in commercialization because of low tap density of nano-sized materials due to high inter-particle repulsion that comes from its high surface area, which makes it difficult to gain high volumetric density of the electrodes.[100,101] It is desirable to use micrometer-sized or submicrometer-sized Si powders for solution of the problem. However, this strategy faces with a dilemma that bigger Si particles bring more severe volume change. Loading high amount of conductive additive helps the Si electrode have stable cycle performance, but lowers the energy density of the electrode due to decrease of the weight of the active material.[102]

Conductive polymer binder playing both roles of conductive additive and polymer binder can be an alternative. In the first part, nano-sized Si electrode that has 3,6-poly(phenanthrenequinone) (PPQ) conductive polymer binder without conventional super P carbon black, which showed superior rate capability to the control and stable cycle performance.[92] However, application of the conductive binder to micro or submicrometer-sized Si is problematic due to its poor adhesion strength. Volume change of nano-sized Si particles is not considerable so that the cycle performance of the Si electrode is stable in despite of poor adhesion property

of binding powders and current collector. This is not in the case, however, binding ability of the binder becomes more critical when the size of the active material is micrometer scale, volume change effect is more severe in bulk size Si powder.

In the second subject of chapter 1, improvement in the performance of the Si electrode with submicro-sized Si powder is showed via compensation of poor adhesion property of PPQ conductive polymer binder by an adhesive binder and the electrode shows better performance compared to using the conventional super P conductive additive. There are some points to be considered. Recently, many researchers reported that the polymer having carboxylic acid groups, for example poly(acrylic acid) (PAA) or carboxymethyl cellulose (CMC), showed good cycle performance in the Si electrodes. This is because of interaction between the polymer binder and Si oxides or silanol groups of the Si surfaces, which make it accommodating the volume change.[66,103] In order to prepare the electrode, polymer binders should be dissolved into proper solvent. Because PPQ binder is dissolved in *N*-methyl-2-pyrrolodione (NMP), compensating binder also should be dissolved in NMP. Among candidates, PAA was selected as a compensating binder due to its solubility in NMP as well as in water.

2.2.2 Experimental

2.2.2.1 Electrode preparation

In order to obtain submicrometerized-Si (SM-Si), Si powder with particle size of 1–5 μm (Alfa Aeasar) was ball-milled using Planetary Micro Mill PULVERISETTE 7 premium line (FSITSCH) for 30 min at Ar atmosphere with a rate of 600 rpm. Morphology of the powders before and after ball-milling were observed using a field-emission scanning electron microscopy (FE-SEM, JEOL JSM-6700F), and the crystal structure of the powders was examined using X-ray diffraction (XRD, D8, Bruker Co., Cu Kα radiation, λ=0.154056 nm). 3,6-Poly(phenanthrenequinone) (PPQ) as a conductive polymer binder was used, synthetic procedure is described in the previous part.

Three different Si electrodes were prepared using various binder composition without conductive additive: weigh ratio of PPQ and poly(acrylic acid) (PAA, Sigma Aldrich, M_v~450000) is 2:1, 1:1, and 1:2. Each polymers were dissolved in *N*-methyl-2-pyrrolidone (NMP) in advance, then two polymer solution were blended according to mixing ratios. Concentration of the composite binder solution was adjusted to 6 wt.%. For the Si/PPQ-PAA composite electrode, SM-Si powder was dispersed into PPQ-PAA composite solution. The resulting slurry was coated on a piece of Cu foil and dried at 120 °C. The loading of PPQ-PAA composite binder was 30 wt.%. To examine the compensation effect of PAA, the Si electrode without PAA, namely PPQ only, was also prepared according to the same procedure described above. The Si electrodes with various composition of PPQ and PAA were named

according to their blending ratio QA21 (2:1), QA11 (1:1), and QA12 (1:2). To compare with the conductive additive-free Si electrode, the electrode with super P carbon black (20 wt.%) and PAA binder (10 wt.%) was prepared. The Si loading in the composite electrode was 0.5–0.7 mg_{Si} cm^{-2}.

2.2.2.2 Measurement of adhesion strength of the electrodes

Adhesion property of the composite binder in the Si electrode was examined via peel test. After cutting the electrode (pressed, 10 μm) into a band 10 cm in width, a piece of polypropylene (PP) film (100 μm thickness) was attached onto the surface of the electrode using a double-sided tape. The ends of the Cu foil and PP film were fixed to tensile stress testing machine (Automatic handy stand, JSV H1000), then forces to peel were measured pulling at a rate of 30 mm min^{-1}.

2.2.2.3 Cell fabrication

Li/SM-Si cells (2032 coin-type) were fabricated to characterize the electrode performance of SM-Si electrodes. To this end, the SM-Si/PPQ-PAA composite electrodes with various composition of PPQ between PAA were loaded into the coin cells along with Li foil. The used electrolyte was 1.3 *M* $LiPF_6$ dissolved in EC/fluoroethylene carbonate (FEC)/DEC (2:2:6, vol. ratio). The PP/PE/PP tri-layer separator (Celgard) was used.

2.2.2.4 Charge-discharge test

The galvanostatic lithiation (charge) and de-lithiation (discharge) cycling of Li/sm-Si cells were conducted using a TOSCAT-3100 (TOYO SYMSTEM CO., LTD.) at 25 °C in a constant current mode. Pre-cycling step was added in order to obtain full activation of Si active material and generation of stable solid electrolyte interphase (SEI) layers on the Si particles. To this end, the galvanostatic charge-discharge cycling was performed 2 cycles. The current density was 100 mA g_{Si}^{-1} for the first cycle and increased to 200 mA g_{Si}^{-1} for the second cycle. The voltage range was 0.005–1 V for the first pre-cycling and 0.07–1 V for the second pre-cycling. Lithiation at the first pre-cycling was conducted with constant current-constant voltage mode (CC-CV), lithiation to the lower cut-off voltage 0.005 V and maintaining of 0.005 V until current drops to 10 mA g_{Si}^{-1}. After lithiation and de-lithiation, charge-discharge tests were rested for 30 min and voltage behavior was monitored.

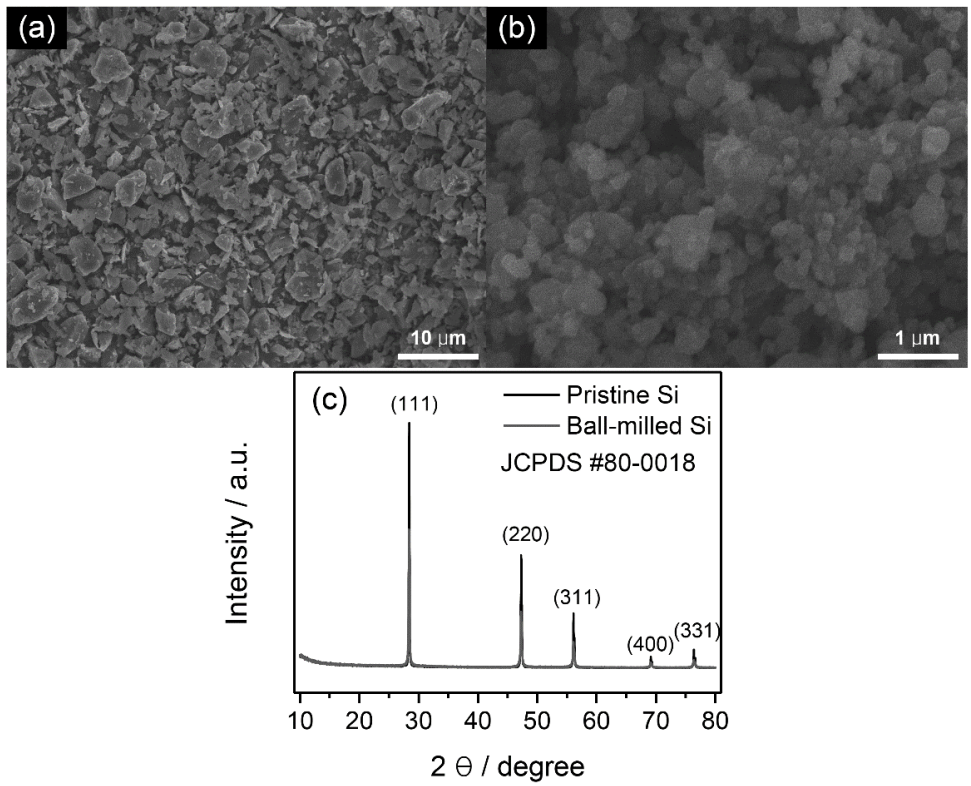

Figure 24. FE-SEM images of (a) pristine Si powder (1–5 μm), (b) ball-milled Si powder (submicrometer-sized). X-ray diffraction patterns of the powders (c). The ball-milling condition is 600 rpm for 30 min at Ar atmosphere.

2.2.3 Results and discussion

It is difficult to use Si raw powders with 1–5 μm size because mechanical stress induced by repetitive volume change of particles during charge-discharge brings particle pulverization or inter-particle electrical contact loss and eventually makes electrically isolated Si particles.[104] To improve this problem, size of Si particles was reduced via mechanical ball-milling. As presented in Figure 24, Si particles with 1–5 μm after ball-milling at Ar atmosphere became smaller, size of 0.2–0.8 μm, and their crystal structure was not changed which examined via comparison with their X-ray diffraction patterns. Decrease of intensity of peaks is due to decrease of crystalline Si by ball-milling.

Cycle performance and voltage profiles of pre-cycling of SM-Si electrode with PPQ binder only is displayed in Figure 25. At the first cycle of pre-cycling, de-lithiation capacity of the electrode is about 700 mA h g_{Si}^{-1}, while lithation capacity reaches to about 4500 mA h g_{Si}^{-1}. From observation of voltage plateau at 0.4 V in Figure 25b, it is confirmed that crystalline $Li_{15}Si_4$ phase was generated at the first lithiation. It seems that most of Li^+ ions and electrons in the lithiated Si particles could not be extracted because that the intensity of the de-lithiation plateau peak is much smaller than the intensity of corresponding lithiation peak. Capacity of the electrode fades very quickly from the first cycle, and is maintained marginal value of below 200 mA h g_{Si}^{-1}. It was seen that the electrode layer was delaminated from the Cu current collector when the cell was disassembled after the first cycling. This implies that there is a problem in the adhesion strength of the PPQ binder to accommodate the volume variation of the SM-Si particles. When the PPQ binder was applied to nanometer-sized Si electrode, severe capacity fading was not

observed, which is probably due to electrochemical and chemical stability of the PPQ binder and absolute volume change of the nanometer-sized Si particles is not big. However, use of SM-Si particles is not in the case because the PPQ binder cannot accommodate the volume variation of the electrode according to the particle size is increased. Although the conductive PPQ binder plays a role of conductive additive, it is hard for the PPQ binder to apply the Si electrodes with the size of bigger than nanometer scale because if its poor adhesion property.

Poly(acrylic acid) (PAA) is introduced to compensate poor adhesion strength of the PPQ binder. It has been reported that cycle performance of the Si-based electrode was considerably improved by introduction of PAA binder, which is due to its superior adhesion property compared to the conventional polymer binder such as polyvinylinene difluoride (PVDF).[65,66] As expected, the adhesion strength of the SM-Si electrode with the PPQ conductive binder was greatly improved by addition of PAA and the results of the peel test of the electrodes with PPQ-PAA composite binder and the PPQ binder only are shown in Figure 26. The adhesion strength of the SM-Si electrode with the PPQ conductive binder is only 0.06 N cm^{-1}. By the way, the adhesion strength of the electrodes with PPQ-PAA composite binder was increased to about 2, 4, 5.5 N cm^{-1}, for 33 % (QA21), 50 % (QA11), and 67 % (QA12) addition of PAA respectively. It is confirmed that PAA provides Si-based negative electrodes with good adhesion property by interactions between carboxylic acid group of PAA and surface functional groups of Si particles. In case of the QA21 having 10 wt.% of PAA in the total electrode, the force to peel the electrode layer from the double-sided tape is similar to that of the reported value.[66]

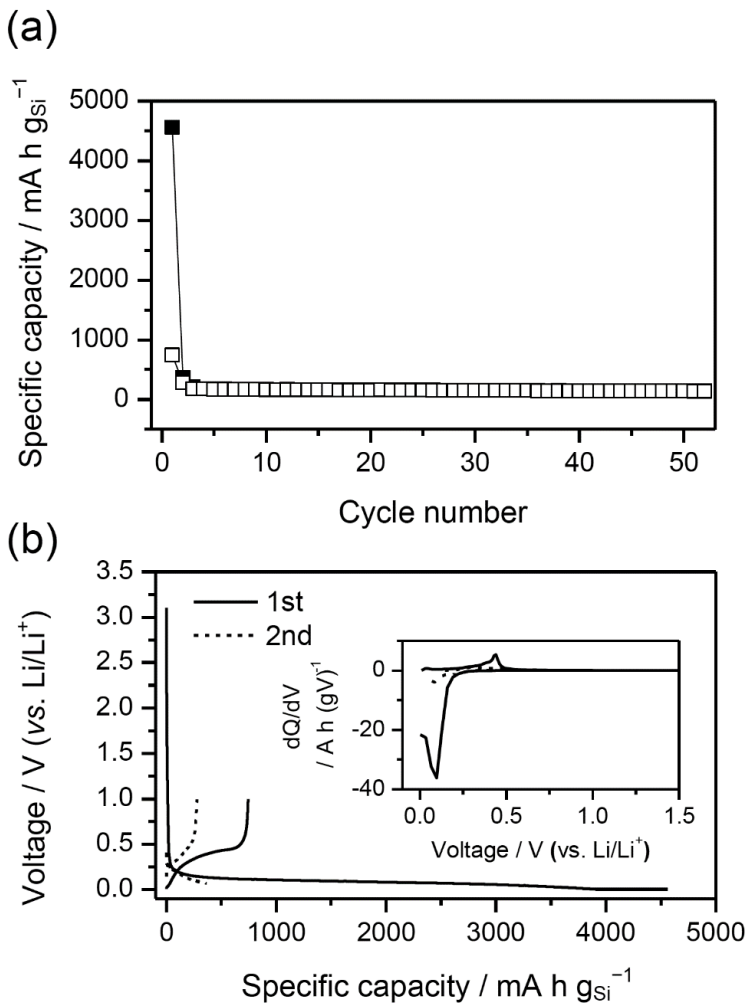

Figure 25. (a) Cycle performance of the Li/Si cell with PPQ conductive binder without conductive additive, (b) the charge/discharge voltage profiles of Li/SM-Si cell at first two pre-cycle. The binder content in the Si electrode is 30 wt.%.

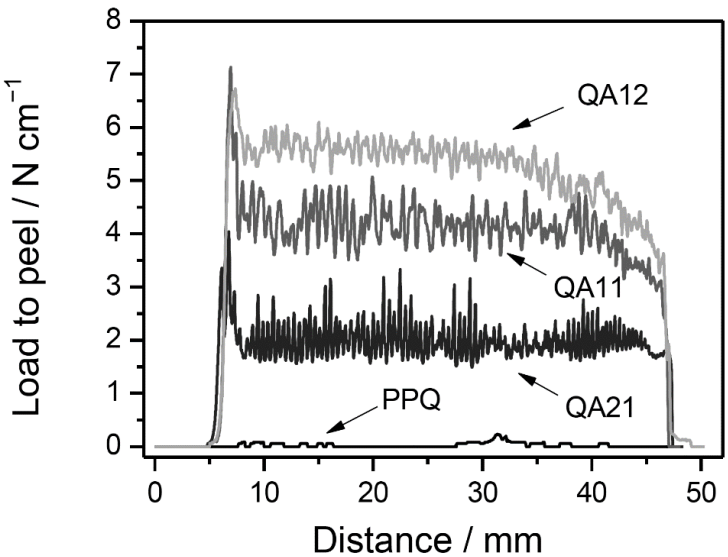

Figure 26. Adhesion strength of the SM-Si electrodes with PPQ-PAA composite binder to the Cu current collector measured by the peel test. Sample name QAxy represents the Si electrode with the PPQ-PAA composite binder with blending ratio x:y. Peel test condition: 30 mm min^{-1}.

Cycle performances of the SM-Si electrodes with the PPQ-PAA composite binder are showed in Figure 27. While the electrode with the PPQ binder shows poor cycleability because of its low binding ability of SM-Si particles and resulted formation of dead particles that are not utilized in electrochemical reaction, the electrodes having PAA as a compensator shows enhanced cycle performance in every blending composition of PPQ and PAA. It is noted that electron transfer among the particles or between particles and current collector is made by the PPQ conductive binder and electrode integrity is maintained by PAA binder. PPQ and PAA are functioning in the composite. Best cycle performance is observed in the condition of blending ratio of 2:1 (67 wt.% of PPQ): 1429 mA h g_{Si}^{-1} at fiftieth cycle. It can be addressed that PAA accommodates effectively the volume change of the Si particles in the electrode with the composite binder as shown adhesion strength results (Figure 26), increased three times from 0.06 N cm^{-1} to 2 N cm^{-1}. However, more PPQ contained in the SM-Si electrode without conductive additive, more stable cycle retention during fifty cycles, which is different trend showed in the adhesion strength results, more PAA, need large force to peel the electrode layer from the current collector. This is consistent with that considerable amount of conductive additive is needed to ensure stable cycle performance of Si negative electrodes in which Si is electrically nonconductor.[102] Although PAA is one of good adhesive polymers so it is expected good binding property in the SM-Si electrode, electrical contacts among Si particles and between the particles and current collector by PAA is limited in the condition of using low content of conductive additive. It can be addressed that the PPQ binder plays a role of conductive additive in the composite electrode to enable the electron transfer in the composite binder of PPQ and PAA.[92]

As shown in Figure 28 the voltage profiles of the electrodes with the PPQ-PAA composite binders along the cycle numbers, differences in the shape of the

voltage profiles are not big, while voltage plateaus around 0.1 V lithiation and 0.3 V de-lithiation of QA11 and QA12 are shifted. In case of QA12, this change in the voltage profiles is more severe that lithiation below 0.1 V is limited so voltage reaches quickly to lithiation cut-off and 0.3 de-lithiation plateau shows considerable polarization. This phenomenon is observed in the differential capacity plot (Figure 29) in detail. First of all, two peaks at lithiation and another two peaks at de-lithation is showed in the plot. Two peaks at de-lithation are originated from de-lithiation of amorphous Si-Li alloy because Si is lithiated down to 0.07 V, in which crystalline $Li_{15}Si_4$ phase is not formed.[84] As seen in Figure 29, differential capacity profiles of QA21 is not changed much but small at lithiation region. On the other hand, two lithiation peaks and two de-lithiation peaks become smaller, and especially 0.3 V de-lithiation peak is shifted to higher voltage in the case of QA11. The fading is more severe in case of QA12: 0.1 V lithiation peak and 0.3 V de-lithiation peak are almost disappeared. Diminished lithiation peaks seems to be related to disappearing of de-lithiation peaks. Decrease of content of conductive additive in micrometer-sized Si electrode makes electrode resistance increase, which results increased polarization during charge-discharge reaction.[102] Therefore when content of the conductive PPQ binder that plays a role of conductive additive is low, there is a problem with lithiation due to increased electrode resistance along cycles.

In order to examine the resistance during lithiation, voltage behavior during 30 min after each lithiation was monitored. Obtained voltage during lithiation with certain current value is called closed-circuit voltage (CCV), and the thermodynamic potential at corresponding state of charge and the polarization are included in this CCV.[104] Current becomes zero during rest period after constant current lithiation. Because polarization is function of current, the thermodynamic potential of the electrode can be obtained after rest period. In this research, stabilized voltage of the

electrode, which approaches thermodynamic value, is called quasi-open circuit voltage (QOCV). Polarization of the electrode is calculated by difference between the lithiation cut-off voltage (CCV, 0.07 V) and QOCV. The internal resistance of the electrode after lithiation is calculated by dividing polarization by applied current value and is plotted versus cycle number in Figure 30. The internal resistance of QA12 that showed capacity drop until fifteenth cycle, shows fixed value after continuous increase until twentieth cycle. Due to this electrode resistance lithiation at low voltage range becomes more and more difficult, which results decrease of reversible capacity. On the other hand, the internal resistance of QA21 is not changed and maintained lowest value along the cycles. This implies that PPQ content in QA21 high enough to ensure electron movement within the electrode, among the particles or between the particles and the current collector.

SM-Si electrode with the PPQ as a polymeric conductive additive shows better cycle performance than that with a conventional particulate conductive additive. To compare with using the polymeric conductive additive, super-P carbon black was used for preparation of the SM-Si electrode. Weight ratio of the components was 7:2:1 for ball-milled Si, super-P carbon black, and PAA binder, respectively (named PAA (7:2:1)). Cycle performances of QA21 and PAA (7:2:1) are displayed in Figure 31a. Cycle retention of QA21 is superior to that of PAA (7:2:1). Interestingly, the two electrodes do not show difference in adhesion strength (Figure 31b). This probably comes from the same content of PAA binder in the Si electrodes. One is the form of polymer, and the other is particulate. Difference in cycle performance should be come from the type of conductive additive. As presented in Figure 31c, the internal resistance measured after each lithiation in case of QA21 is lower than that of PAA (7:2:1). Conventional particulate conductive additive can be aggregated or moved from initial position in the electrode,[105] so

electrical network becomes loosen by poor contact between the Si particles while PPQ co-exists in the composite with PAA binder to form a uniform distribution in the electrode and results lower electrode resistance along the cycles.

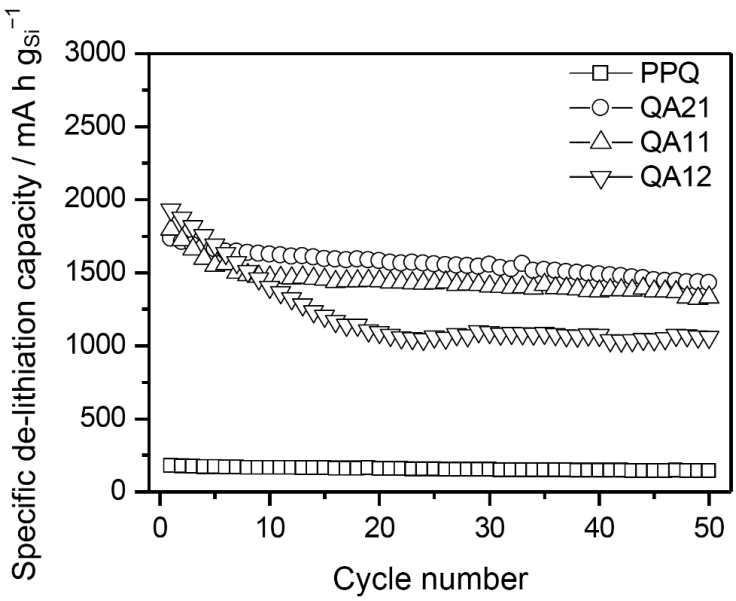

Figure 27. Cycle performance of Li/SM-Si cell with various composite binder (pre-cycling data are excluded) without conductive additive. The binder content in the Si electrode is 30 wt.%. Sample name QAxy represents the Si electrode with the PPQ-PAA composite binder with blending ratio x:y.

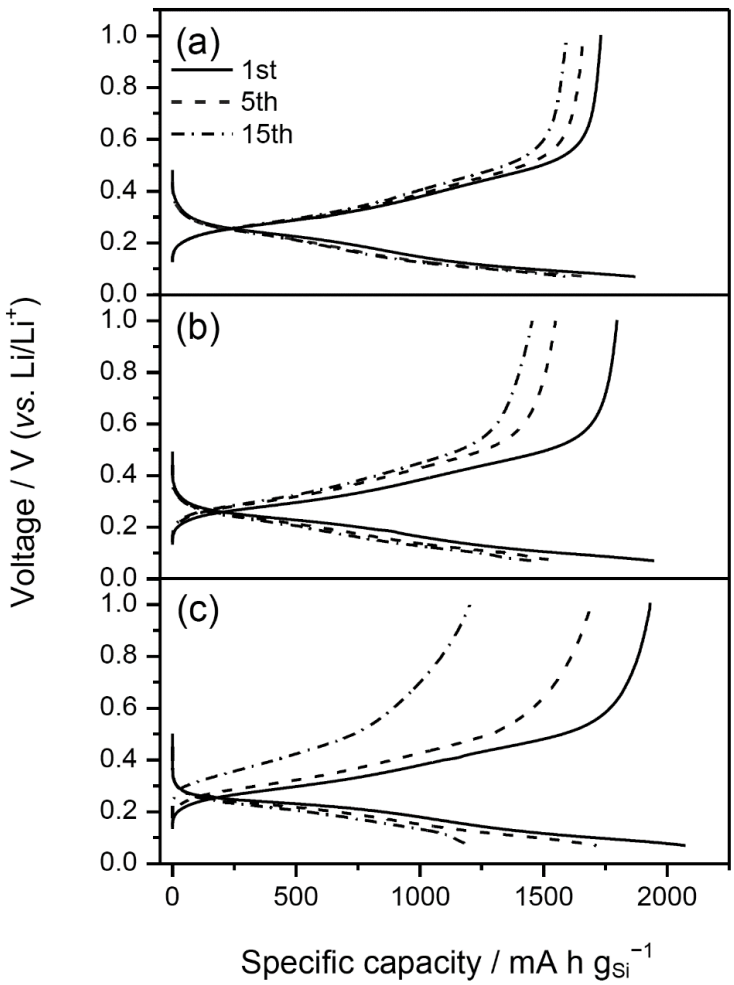

Figure 28. The voltage profile of Li/sm-Si cells at 1st, 5th, and 15th cycle with PPQ-PAA composite binder blended in ratio (a) 2:1, (b) 1:1 and (c) 1:2.

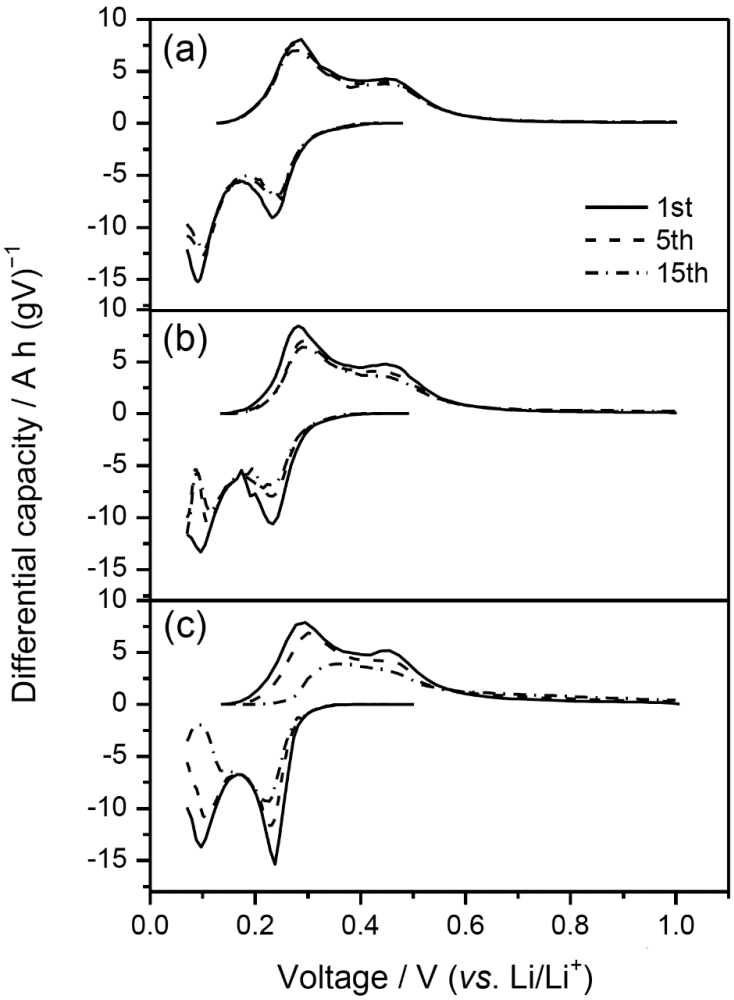

Figure 29. Differential capacity plots of the charge-discharge voltage profiles displayed in Figure 28.

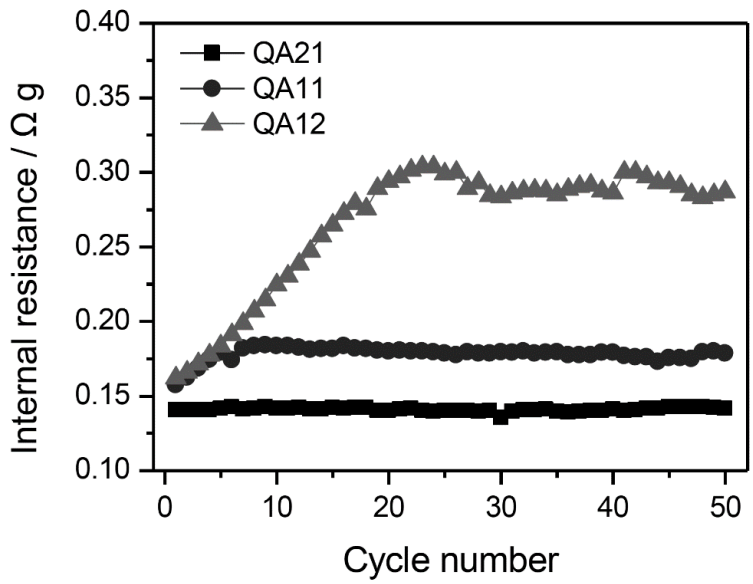

Figure 30. The evolution of the internal resistance of the lithiated electrodes with the composite binders at each cycle derived from difference between charge cut-off voltage (0.07 V) and quasi-open circuit-voltage (QOCV).

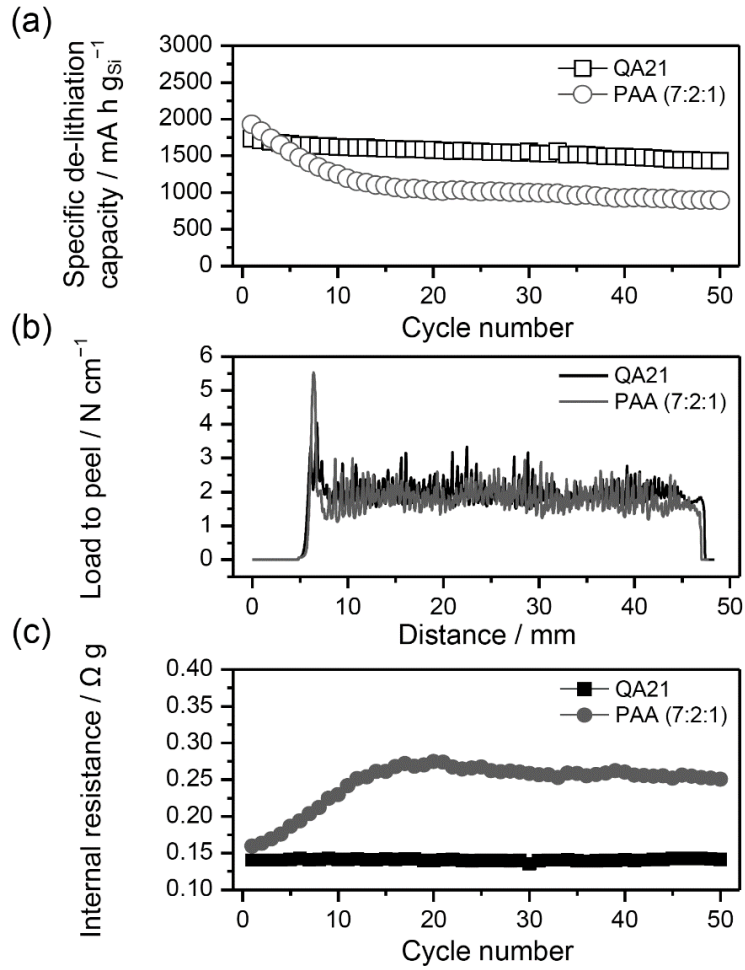

Figure 31. (a) Cycle performance of Li/SM-Si cell with PPQ-PAA (2:1) composite and PAA binder without conductive additive, (b) the corresponding adhesion strength of the Si electrodes with PPQ-PAA (2:1) composite and PAA binder to the Cu current collector measured by the peel test, (c) the evolution of internal resistance of the lithiated electrodes at each cycle derived from difference between charge cut-off voltage (0.07 V) and quasi-open circuit-voltage (QOCV). PAA (7:2:1) means the electrode with the composition of Si : super-P : PAA = 7 : 2 : 1 (by weight).

3. Li^+ ion conductive polymer binder for $LiFePO_4$ positive electrode

3.1 Electrochemical analyses of the $LiFePO_4$ electrode with Li^+ ion conductive poly(acrylic acid) lithium salt binder

3.1.1 Motivation and objectives

Compared with a very conventional positive electrode material such as $LiCoO_2$, olivine-type $LiFePO_4$ has been attracted much attention due to its high theoretical capacity (170 mA h g^{-1}), environmental friendliness, cost competitiveness, structural stability, and thermal stability.[31-33] Due to its great advantages, $LiFePO_4$ has been considered as a power sources of electric vehicles or power tools in which reliability regarding high capacity and cycleability are strongly demanded. However, some problems should be solved. As typical voltage profiles of Li/$LiFePO_4$ cell at high current charge and discharge are shown in Figure 32, higher polarization is observed in the voltage plateau regarding two phase reaction.[106] This problem comes from the fact that lithium diffusion in the crystal structure is slow due to its one-dimensional path and electronic conductivity is low because of its chemical structure containing PO_4^{2-} polyanion.[35] In order to improve power capability of $LiFePO_4$ electrode, down-sizing of $LiFePO_4$ particles with nanometer-scale has been tried for a better lithium diffusion within the particle and coating with carbon materials on the

surface of the $LiFePO_4$ particles to obtain improved electronic conductivity between the $LiFePO_4$ particles and the current collector.[33,34,36,107] Makers of the $LiFePO_4$ powder adopted these strategies and have been produced carbon coated nano-$LiFePO_4$ powders.

In a view point of electrochemistry, a further improvement can be considered. In a discharge reaction of a positive electrode material, Li^+ ions as well as electrons are involved in the reaction. But many researches has been focused on the reaction occurred in a view of the active material particle. To this end, minimization of the particle for higher lithium diffusivity and surface carbon coating have been tried as mentioned above. But, it is noted that the electrochemical reactions involving both Li^+ ions and electrons are firstly occurred in the interface between the surface of the active material and the electrolyte.

Based on this consideration, adoption of a Li^+ conductive polymer binder was considered. It was expected that Li^+ ion transfer from the electrolyte to the surface of $LiFePO_4$ particles can be aided by the Li^+ conductive polymer binder. As a candidate, water-soluble poly(acrylic acid) (PAA)-based binder was selected. PAA has been attracted much attention because electrode preparation process is environment-friendly compared with conventional *N*-methyl-2-pyrrolidone (NMP)-based process. Some researches about using PAA or poly(acrylic acid) lithium salt (LiPAA) for a binder of $LiFePO_4$ positive electrode were reported.[73,74,108] The authors argued that capacity and rate capability of the $LiFePO_4$ electrode with PAA or LiPAA were enhanced due to ionic characteristics of PAA or LiPAA compared with a conventional binder polyvinylidene fluoride (PVDF). Because electron conduction pathways within the electrode become loose when the PVDF binder is swelled in the organic solvents and this can affect the rate capability of the $LiFePO_4$ electrode.[65,109,110] It seems not appropriate to use the PVDF binder as a control group.

LiPAA and PAA were selected as a Li^+ ion conductive and a control group, respectively.

In the second chapter, fast discharge property of the $LiFePO_4$ positive electrode with Li^+ ion conductive LiPAA binder are evaluated electrochemically. To this end, some requirements should be considered. Fast charge and discharge of the electrode are related with charge transfer kinetics accompanied with electron and Li^+ ion transport in the surface of the active material. To investigate the effect of Li^+ ion conductive binder that is present on the surface of $LiFePO_4$ particles, contribution of the electron conduction within the electrode to the rate capability needs to be same whether the binder is Li^+ ion conductive or not. The factors affecting the electron transfer are amount of conductive additive in the electrode, electrode thickness, active material loading level, and so on. In addition, electrode porosity should be controlled because Li^+ ion transport to the surface of active material is occurred in the impregnated electrolyte.

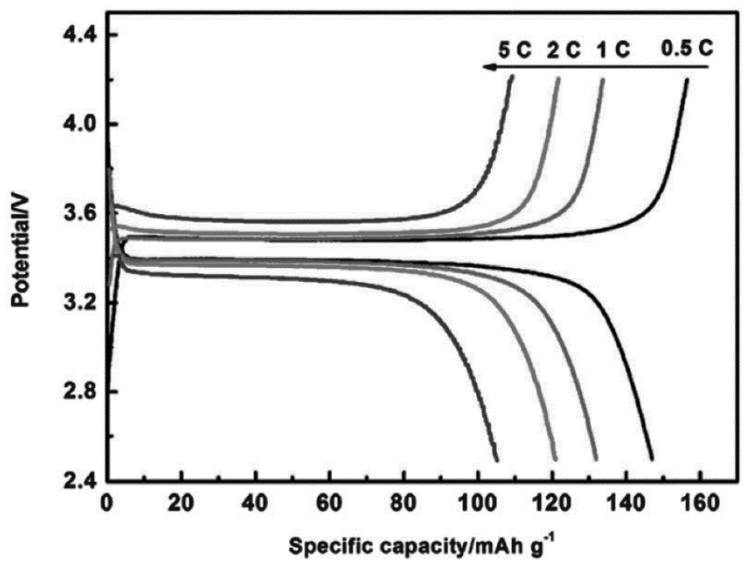

Figure 32. An example of charge-discharge voltage profiles of Li/$LiFePO_4$ cell at different current densities.[106]

3.1.2 Experimental

3.1.2.1 Preparation of electrode

$LiFePO_4$ powder that is provided by EIG company for free was used as an active material. By observation with FE-SEM, size of particles is 100–400 nm and typical particle shape is elliptical (Figure 33). Surface of the $LiFePO_4$ is coated with carbon layer of ~10 nm, which is confirmed with high resolution transmission electron microscope (HR-TEM, JEM-3010), and carbon content in the total power weight is about 2.2 %, which is confirmed with elemental analyzer (Flash1112, Flash2000). X-ray diffraction (XRD) pattern of the powder was obtained with a diffractometer (D8, Bruker Co., Cu Kα radiation, $\lambda = 0.154056$ nm) to show high crystalline phase. For preparation of the composite electrode, $LiFePO_4$ powder and super-P conductive additive were dispersed in the binder solutions, which are prepared by dissolving of poly(acrylic acid) (PAA) and its Li salt (LiPAA) prepared with LiOH in water. Electrode composition of the active material, super-P, and the binder was 90:3:7 by weight. The resulting slurry was coated on a piece of Al foil and dried at 60 °C 30 min. After pressing using a roll-presser, electrode sheet was punching in a disk shape with diameter of 1.1 cm and further vacuum-dried at 100 °C overnight. $LiFePO_4$ loading was 2.6–2.7 mg cm^{-2}, and the porosity of the electrode was adjusted to about 30 %. Electronic conductivity of the electrode with the two binder measured using 4-point probe method was 4.7×10^{-3} and 4.4×10^{-3} S cm^{-1} that are similar each other.

3.1.2.2 Cell fabrication

$Li/LiFePO_4$ half-cells (2032 coin-type) were fabricated to characterize the electrode performance with PAA and LiPAA binders. To this end, the $LiFePO_4$/PAA and $LiFePO_4$/LiPAA composite electrodes were loaded into the coin cells along with Li foil. The used electrolyte was 1.0 *M* $LiPF_6$ dissolved in EC/DEC (1:1, vol. ratio). The PP/PE/PP tri-layer separator (Celgard) was used. To investigate the effect of salt concentration, the electrolyte with 0.5 *M* $LiPF_6$ in EC/DEC (1:1, vol. ratio) was prepared and used in the cell fabrication.

3.1.2.3 Electrochemical characterization

3.1.2.3.1 Charge-discharge test

The galvanostatic charge (de-lithiation) and discharge (lithiation) cycling of $Li/LiFePO_4$ cells was conducted using a TOSCAT-3100 (TOYO SYMSTEM CO., LTD.) at 25 °C in a constant current mode. Pre-cycling step was added in order to obtain full activation of $LiFePO_4$. To this end, the galvanostatic charge-discharge cycling was performed 3 cycles. The current density was 0.1 C-rate and 0.2 C-rate for the pre-cycling and cycling, respectively (1 C-rate is 170 mA g^{-1}). The voltage range was 2.2–4.2 V. To confirm the rate capability of the $LiFePO_4$ electrode with the two binders, discharge current was variated as 0.2, 2, 10, and 30 C while charge

current was fixed to 0.2 C.

3.1.2.3.2 Galvanostatic polarization of symmetrical lithium metal cell

In order to confirm the Li^+ ion conductive feature of PAA and LiPAA, a galvanostatic polarization test was conducted using a symmetrical lithium metal cell. PAA and LiPAA aqueous solutions were poured on a silicone rubber mold that was attached to a piece of polypropylene sheet. After drying at 60 °C for 1 h, detached films were punched into disk shape of 1.9 cm diameter. The polymer films were dried in a vacuum oven at 100 °C overnight, and stored in the electrolyte in a glove box until use. Their thickness was in range of 70–80 μm. PAA and LiPAA films were sandwiched by two lithium metal disk of 1.1 cm diameter in a coin cell. 1 *M* $LiPF_6$ in EC/DEC (1:1, vol. ratio) was used as an electrolyte. After cell assembly and stabilization in a temperature-controlled oven, current pulses of 1, 2, 3, 4, and 5 μA cm^{-2} was induced for 1 h. Between each current polarization, the cell was rested for 1 h.

3.1.2.3.3 Electrochemical impedance spectroscopy (EIS)

To confirm the difference in the impedance of the $LiFePO_4$ electrode with PAA and LiPAA binder, AC impedance of the cells were measured using Electrochemical Workstation (CH Instrument). For more precise measurement, EIS was conducted with symmetrical cells. After three cycles, Li/$LiFePO_4$ half-cells were charged to 4.2

V with 0.1 C and maintained at 4.2 V until current drop to 0.01 C (constant current-constant voltage mode). The cells were disassembled and charged electrodes were cut into two parts with same area. Each electrode was sandwiched and separated by a piece of PP/PE/PP separator. After stabilization overnight, EIS measurements were performed with frequency range of 100 kHz–5 mHz and a 5 mV amplitude.

3.1.2.3.4 Spectroscopic analysis

Identification of the carboxylic acid group and carboxylate anion in PAA and LiPAA, Fourier transform infrared spectroscopy (FT-IR) measurements were conducted with attenuated total reflectance mode (Ge window) using a spectrophotometer (Thermo Scientific, Nicolet 6700, USA). To confirm whether carboxylic acid group of PAA is converted to carboxylate anion in the electrolyte or in the condition of cycling, FT-IR spectra of film electrodes of PAA (PAA was coated onto Al foil) that were soaked in the 1 *M* $LiPF_6$ in EC/DEC (1:1, by vol.) for three days or cycled using cyclic voltammetry in the voltage range of 2.2–4.2 V were collected.

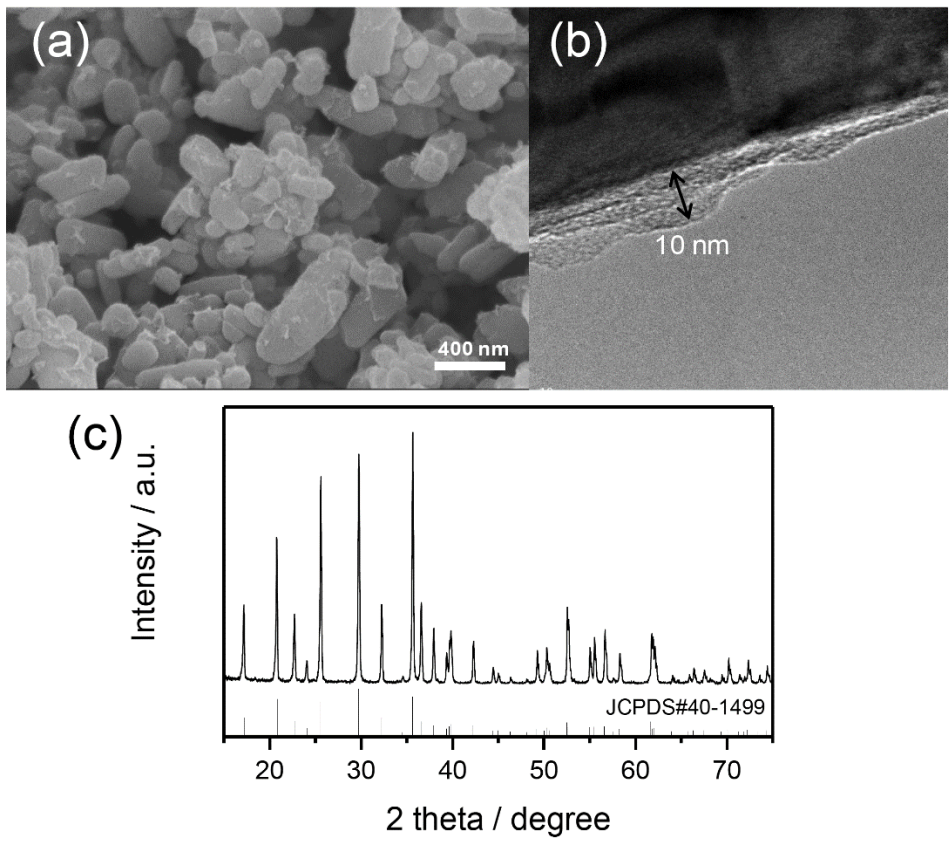

Figure 33. (a) FE-SEM image of $LiFePO_4$ powder, (b) TEM image of a carbon-coated $LiFePO_4$ particle, thickness of the carbon layer is around 10 nm, (c) XRD pattern of $LiFePO_4$ powder.

3.1.3 Results and discussion

Protons in bare PAA is not easily dissociated from the carboxylic acid group because the carboxylic acid is a weak acid. By the way, in neutral pH, PAA loses its protons and acquires negative charges, carboxylic anions. So PAA has been used as a polyelectrolyte.[111] In Figure 34, while asymmetrical and symmetrical stretch vibrations attributed to C=O of the carboxylate anion are observed in 1549 and 1408 cm^{-1}, respectively.[112,113], stretch vibration attributed to C=O of the carboxylic acid group is observed in 1694 cm^{-1} even the PAA film is soaked in the electrolyte or cycled in voltage range of 2.2–4.2 V. From this observation, PAA is not converted to the salt form, carboxylate anion, in the environment of the cell. So LiPAA is used for a Li^+ conductive polymer binder and PAA is used for a control.

As presented in Figure 35, both $LiFePO_4$ electrodes with the PAA and the LiPAA binder shows excellent cycle retention above 99 % at fiftieth cycle. This might due to the well-maintained electrical network of the $LiFePO_4$ electrode during the cycling. It was previously reported that cycle performance of the $LiFePO_4$ electrode prepared with PAA binder was superior than that of the electrode with a conventional binder, polyvinylidene difluoride (PVDF). Main reason is that PVDF is easily swelled in the organic electrolyte while PAA is not, which results weakened or broken electrical network in the electrode because binding property was damaged.[74] There is a difference, however, in the shape of voltage profiles between the electrode with the PAA and the LiPAA. As displayed voltage profiles at the first cycle and the fortieth cycle are presented in Figure 35b and 35c, some polarization at the end of charge and discharge in the electrode with PAA binder compared to the that of the electrode with the the LiPAA binder. This trend is observed at the fortieth

cycle as well as the first cycle. There might be a difference in the kinetic properties between the two electrodes, namely Li^+ ion conductive nature of the binders.

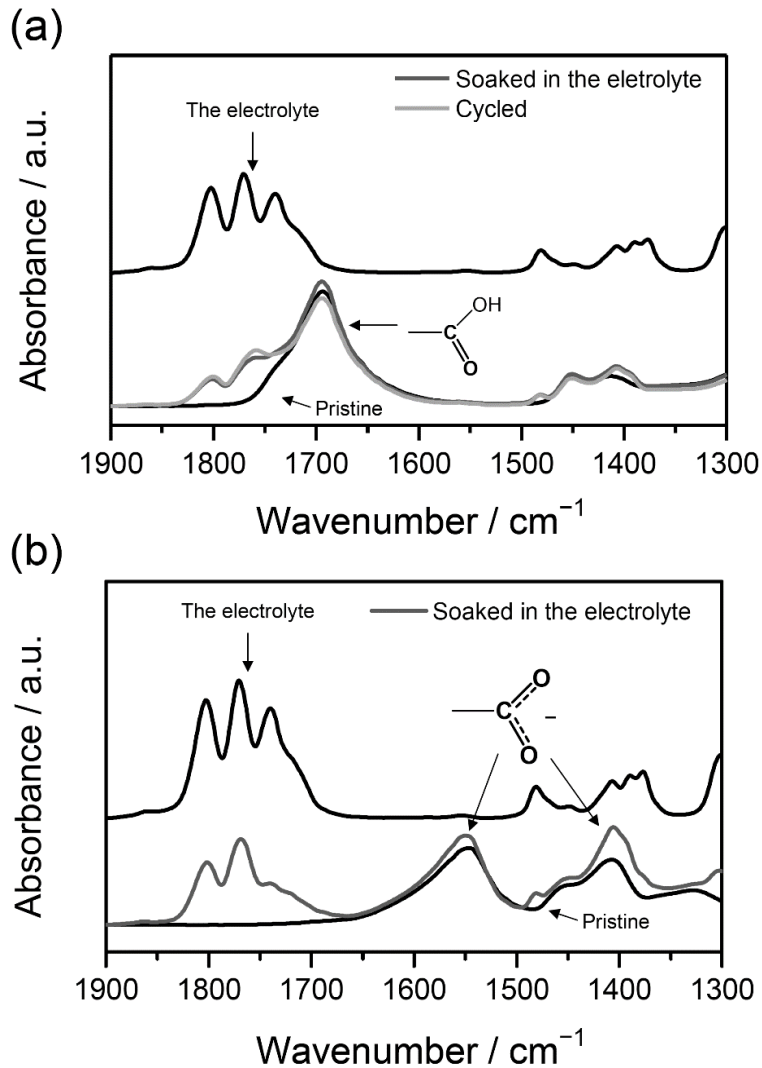

Figure 34. FT-IR spectra of (a) PAA film and (b) LiPAA film coated on a piece of Al foil, respectively. To confirm the possibility of change of carboxylic acid of PAA to carboxylic acid Li salt, spectra of the PAA film electrodes that were stored in the electrolyte or cycled via cyclic voltammetry were also obtained.

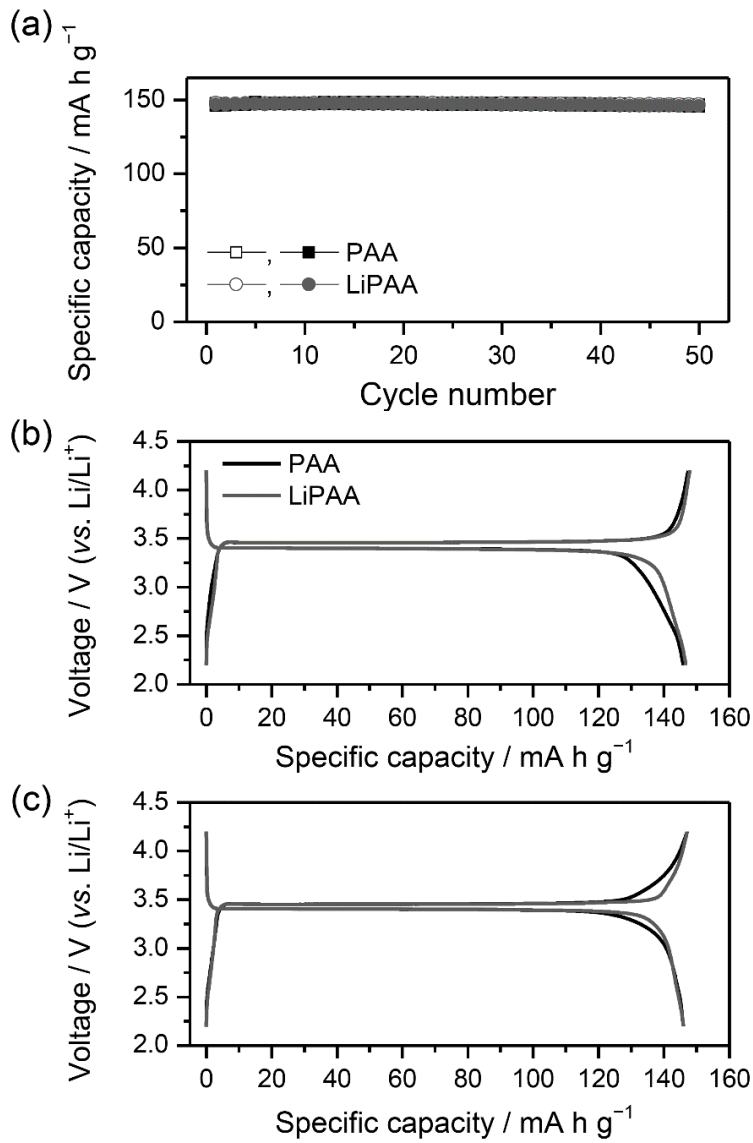

Figure 35. (a) The charge-discharge cycle performances of Li/$LiFePO_4$ cells (pre-cycling data are excluded), in which the working electrodes are fabricated with the PAA and LiPAA binder and the voltage profiles at the first cycle (b) and the fortieth cycle.

To confirm the effect of Li^+ ion conductive properties in fast electrochemical reaction, rate capability of the $LiFePO_4$ electrode with the PAA and the LiPAA binder was examined (Figure 36). At 0.2 C discharge, capacity is same between the electrode with the PAA and the LiPAA, 145.7 mA h g^{-1}, but polarization at the end of discharge is observed in case of PAA binder as also seen in Figure 35. As discharge current becomes higher, discharge capacity of the electrode with the PAA becomes smaller than that of the electrode with the LiPAA. At 2 C discharge, capacity values of the electrode with the PAA and the LiPAA are 129.7 and 137.5 mA h g^{-1}. Differences in discharge capacity values at larger C-rate become bigger, 99.4 mA h g^{-1} versus 118.2 mA h g^{-1} for 10 C. Moreover, larger polarization at the main discharge reaction plateau of $LiFePO_4$ is observed compared to the electrode with the LiPAA. Polarization is defined as a difference between the QOCV voltage plateau and the voltage plateau at each discharge current.[104] For detailed explanation about QOCV, see the chapter 1. Polarizations of the electrode with the PAA are 0.03, 0.11, and 0.27 V for 0.2 C, 2 C, and 10 C, respectively. In case of the electrode with the LiPAA, less polarization is induced: 0.02, 0.05, and 0.15 V for 0.2 C, 2 C, and 10 C, respectively. Since electronic conductivity of the electrode with the two binder was similar, rate capability of the electrodes should be limited due to the difference in Li^+ ion transfer kinetics in the interface between the active material and the electrolyte, e.g. kind of the binder. It is noted that the activation energy for the charge transfer at the positive active material/electrolyte interface is influenced with their interphase material.[114] If the binder at the interface between the $LiFePO_4$ and the electrolyte is conductive for the Li^+ ions, an expectation that charge transfer in the interface is compensated by the conductive binder in the high discharge condition is quite reasonable.

To highlight the effect of the Li^+ ion conductive LiPAA binder, a

potentiostatic polarization experiment was conducted (Figure 37). After $LiFePO_4$ electrodes with the PAA and the LiPAA binder were pre-cycled, state of charge of the cells were adjusted to 50 %. After stabilization of the cell voltage (3.42 V), voltage of 2.2 V was applied to the cells, which is the lower voltage cut-off. Because of the applied potential is lower than the cell voltage, an instantaneous lithiation reaction is occurred to meet the polarizing potential. In this situation, Li^+ ions in the bulk electrolyte is diffused to the surface of $LiFePO_4$ particles. It is expected that because the binder films are in the interface between the active material and the electrolyte, the transfer of Li^+ ions are affected by the kind of the binders. As shown in Figure 37b, the currents exponentially decay with the times. By the way, a difference in the peak current is observed after instantaneous potential step. Larger current is passed through the cell with the electrode with the LiPAA binder compared with the electrode with the PAA binder. Showed peak currents in the electrode with the PAA and the LiPAA are −21.6 and −35.4 mA, respectively. This implies that Li^+ ion transfer in the interface between the surface of $LiFePO_4$ and the electrolyte is faster in case of the LiPAA binder. In other words, Li^+ ion transfer is more favorable in the interface, in which the LiPAA binder covers the surface of $LiFePO_4$ particles. Li^+ ion conductive property of the binders that cover the surface of the $LiFePO_4$ particles can be estimated by a galvanostatic polarization experiment described in Figure 38a. To confirm the polarization to the transfer of Li^+ ions, a symmetrical cell in which polymer binder film is sandwiched by two lithium metal electrode was constructed. When an oxidation current pulse is applied to a lithium metal electrode A, Li^+ ions are generated by oxidation and go to the opposite lithium metal electrode B through the polymer film. With the voltage response according to the applied current steps, polarization to the transfer of Li^+ ions can be obtained. As shown in Figure 38b, higher polarizations with the current pulses are observed in the PAA film.

At applied the current pulses of 1, 2, 3, 4, and 5 μA cm^{-2}, the polarizations are 0.947, 1.900, 2.876, 3.876, and 4.885 V, respectively while the polarizations in case of the LiPAA film are 0.005, 0.011, 0.018, 0.022, and 0.028 V, respectively. This implies that Li^+ ion transfer through the PAA film is more difficult than the LiPAA film. Li^+ ion transfer through PAA film layer that is present on the surface of the active material is more difficult. Discharge property at low discharge current rate is not problematic, for the surface coverage by the binder is not perfect and the Li^+ ion transfer can be occurred in the bare surface of the active material. However, this becomes problematic when high rate of discharge current is applied to the electrode. Fast accessibility of the Li^+ ions from the bulk electrolyte to the surface of $LiFePO_4$ particles is hindered by PAA film layer. In other words, discharge rate capability of the electrode with the PAA binder is limited because of smaller surface area in which Li^+ ions can be accessed.

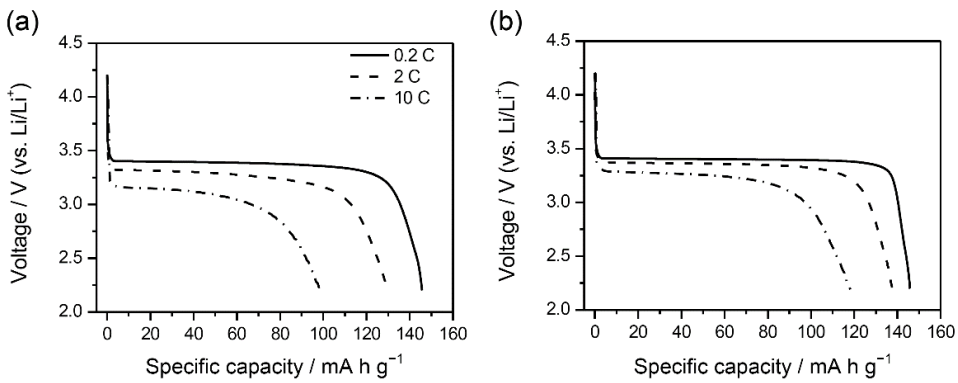

(c)

	$(QOCV_{discharge} - V_{discharge})(V)$		
	0.2 C	2 C	10 C
LFP-PAA	0.03	0.11	0.27
LFP-LiPAA	0.02	0.05	0.15

Figure 36. The charge-discharge voltage profiles of Li/$LiFePO_4$ cells in which the $LiFePO_4$ electrode fabricated with PAA binder (a) and LiPAA binder (b). (c) Polarization at each discharge rate is calculated with the difference between quasi-open-circuit voltage at discharge plateau and discharge voltage plateaus (closed-circuit voltage).

This effect can be further confirmed by a discharge rate capability test with the cells in which the electrolyte with lower salt concentration is injected. Ionic conductivity (σ) of a electrolyte is defined as $\sigma = F\sum_i |z_i| u_i c_i$. F, z_i, u_i, and c_i are Faraday constant, charge of the ionic species, mobility of the ionic species, and concentration of the ionic species, respectively. If the concentration of the salt is decreased, ionic conductivity is decreased by the above relation. Discharge rate capability tests with the cells in which the electrolyte of 0.5*M* $LiPF_6$ salt is dissolved in the mixture of EC and DEC (1:1 by vol.) is injected. As shown in Figure 39, discharge capacities of the electrode with the LiPAA are higher than the electrode with the PAA at higher discharge current. This difference can be explained as follows. The surface of the $LiFePO_4$ particles are covered by the LiPAA binder in which lithium salt form of carboxylate anion is present. Li^+ ions are migrated to the surface of $LiFePO_4$ active material by galvanostatic discharging current. In this situation, Li^+ ions that are migrated to the $LiFePO_4$ were the Li^+ ions that were bound to the carboxylate anion before discharge reaction. To satisfy the electroneutrality of carboxylate anion, Li^+ ions should be provided from the outer electrolyte, in other words, forced transport of the Li^+ ions is occurred. PAA does not have this function, so the discharge rate capability becomes poorer with the electrolyte of 0.5*M* $LiPF_6$ concentration. But, in case of the LiPAA binder, lowered conductivity of Li^+ ions are compensated in the interface by this function, so high rate discharge capacities with lower salt concentration is similar with that with 1.0 *M* $LiPF_6$ electrolyte.

Electrochemical impedance results of the electrode with the two binders are shown in Figure 40. In order to eliminate of the effect of lithium metal counter and reference electrode, symmetrical cells were fabricated. The experimental data were fitted with an equivalent circuit that is presented in the Figure 40c. Two semicircles are observed in both electrodes with the PAA binder and the LiPAA binder. The

semicircles at higher and lower frequency are related to a resistance of surface film and a resistance in the charge transfer, respectively. A resistance at most high frequency means sum of the resistance of the electrolyte and ohmic resistance of the electrode. The two electrodes do not show big differences in R_{Ω} and R_{film}. However, charge transfer resistance of the electrode with the PAA binder is three times higher than that of the electrode with the LiPAA binder. This implies that it can be considered that charge transfer reaction is occurred in the interface between the active material and the electrolyte, so the LiPAA binder that is present in the interface seems to aid the charge transfer by assist of Li^+ ion transfer. According to a previous report[115], negatively polarized oxygen in the carboxylate group attracts Li^+ ions that are solvated by solvent molecules, so de-solvation of Li^+ ions are facilitated. By this consideration, it can be said that Li^+ ions are more friendly with carboxylate anions in LiPAA than carboxylic acid group in PAA because carboxylate anion has negative charge. Due to the lower charge transfer resistance at higher current discharge in the electrode fabricated with LiPAA binder, better discharge rate capability can be obtained.

Improved discharge rate capability of the $LiFePO_4$ electrode with the LiPAA can be explained with a schematic diagram that is shown in Figure 41. At a condition of fast discharge reaction, Li^+ ion transfer in the interface between the active material and the electrolyte limits the total reaction. If the binder that covers the surface of $LiFePO_4$ particle, actually, the surface that is not covered by the binder may be there, Li^+ ion transfer from the electrolyte to the surface of $LiFePO_4$ is assisted by Li^+ ion conductive LiPAA binder. Because the accessible sites of the Li^+ ions are more in the surface of the electrode with the LiPAA binder, Li^+ ions that can be participated in the reaction are more even in the condition of fast discharge current.

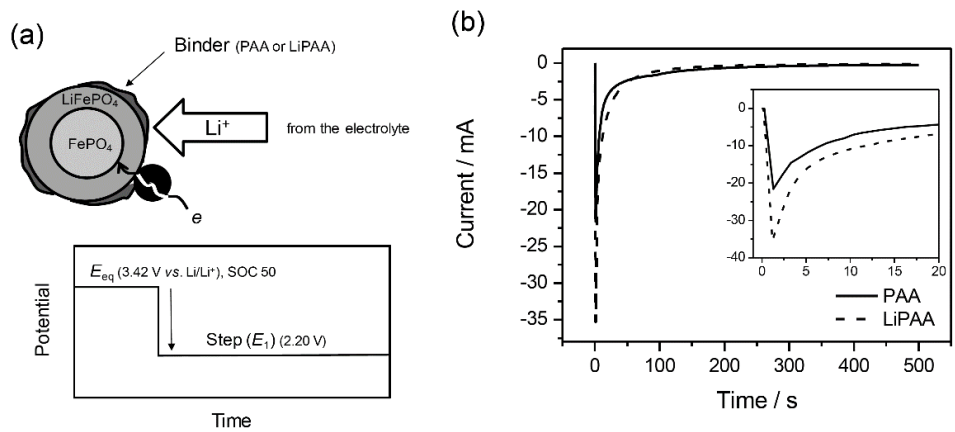

Figure 37. Potentiostatic polarization of Li/$LiFePO_4$ cells. (a) Experimental concept and (b) current behavior during potential step.

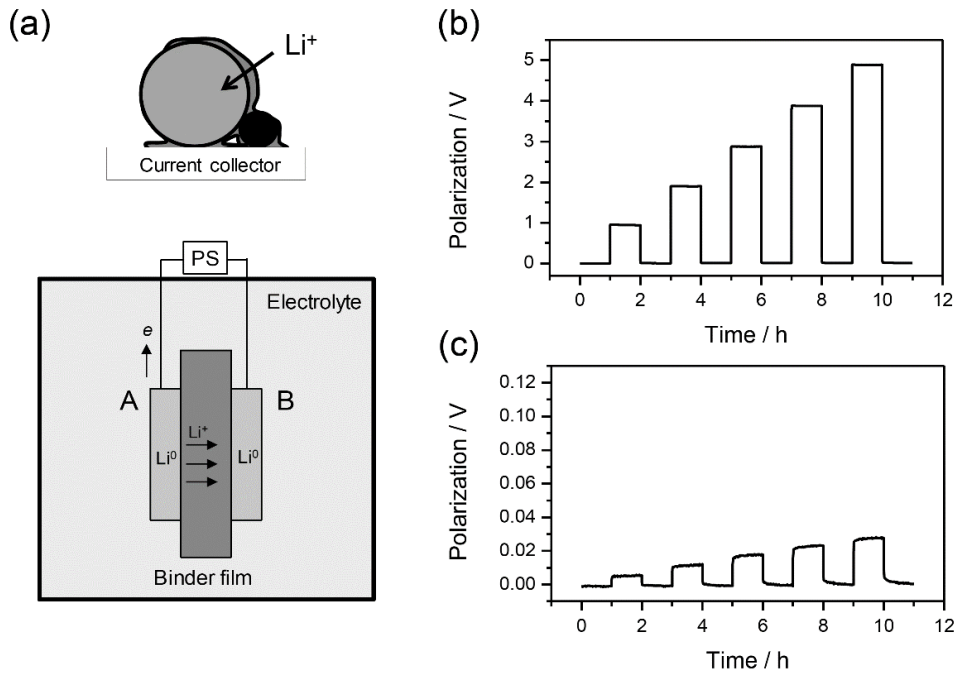

Figure 38. Galvanostatic polarization of Li/binder film/Li symmetrical cell. (a) Concept of the experiment and polarization behavior of the cells with PAA film (b) and LiPAA film (c). Thickness of the films is 70–80 μm.

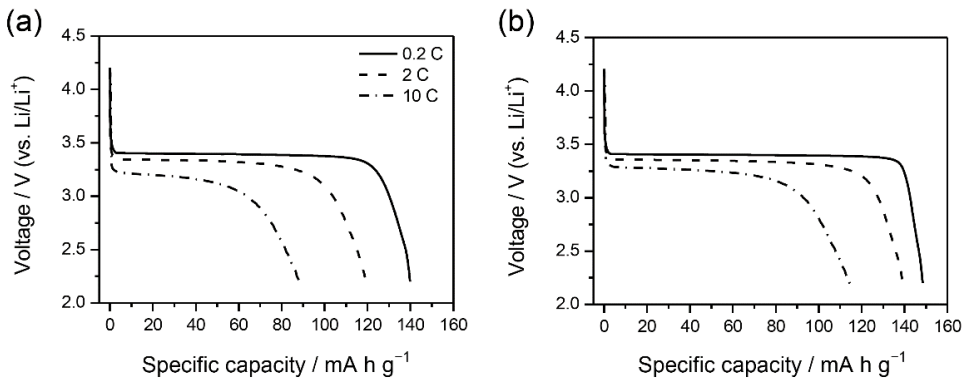

Figure 39. The discharge voltage profiles of Li/$LiFePO_4$ cells with various discharge current, in which the electrolyte with 0.5 *M* $LiPF_6$ salt concentration is used. (a) PAA binder, (b) LiPAA binder.

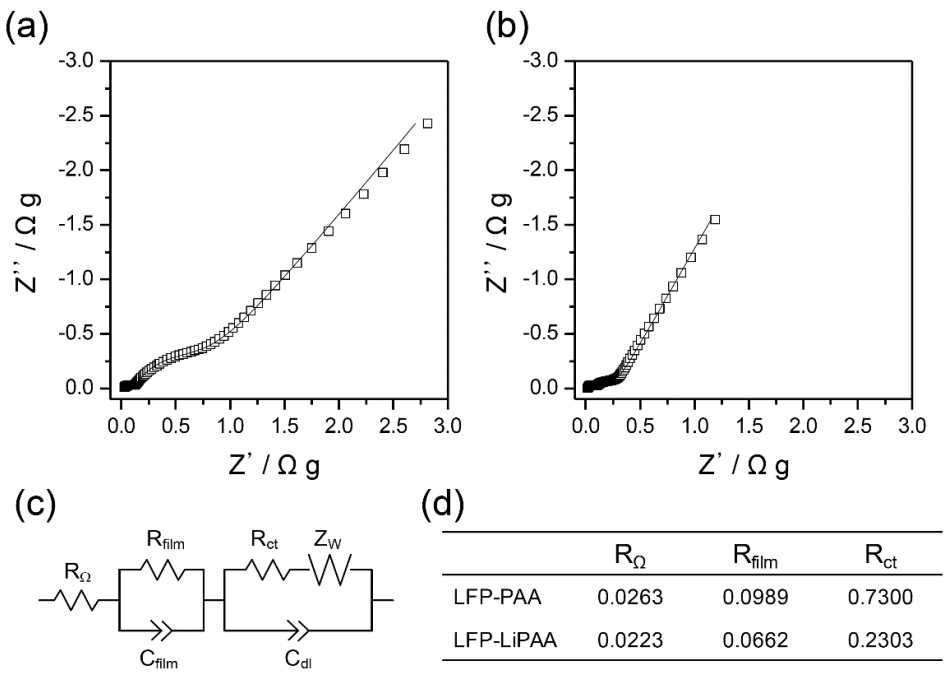

	R_Ω	R_{film}	R_{ct}
LFP-PAA	0.0263	0.0989	0.7300
LFP-LiPAA	0.0223	0.0662	0.2303

Figure 40. AC impedance spectra of $LiFePO_4$ symmetric cells, for $LiFePO_4$ electrodes fabricated with PAA (a) and LiPAA (b). (c) Equivalent circuit for fitting and (d) fitting results.

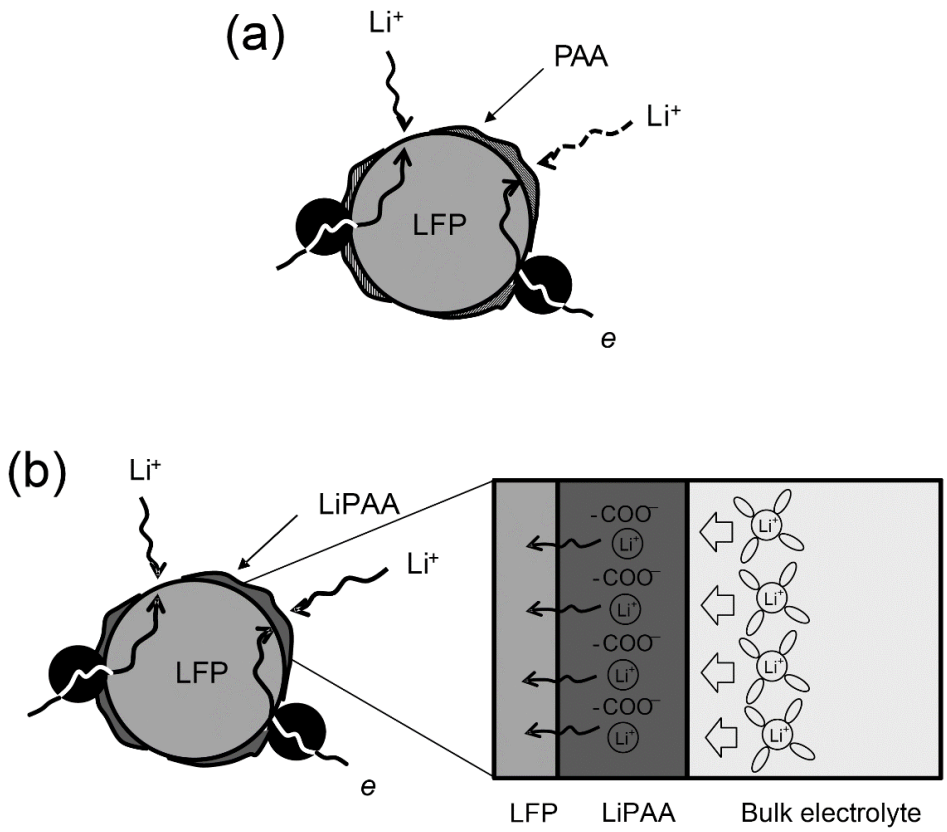

Figure 41. Schematic representation of $LiFePO_4$ electrode with PAA binder (a) and LiPAA binder (b).

4. Conclusions

In this study, the effects of using electronic or Li^+ ion conductive polymer binder for Si negative electrode or $LiFePO_4$ positive electrode are investigated.

Firstly, a conductive polymer 3,6-poly(phenanthrenequinone) (PPQ) is applied to the nano-sized Si electrode and tested whether the PPQ could act as a conductive additive. The PPQ binder that is formulated with nano-sized Si powder without conventional conductive additive (super P) is reduced (n-doped) to be a mixed conductor (both electronic and Li^+ ion conductor) during the first lithiation period. The binder is electronically conductive in the working potential of Si (0.0–0.5 V). The PPQ binder is uniformly dispersed within the nano-Si composite electrode to effectively convey electrons from Si to the current collector. The loading of PPQ can be minimized down to 10 wt.%.

Secondly, in order to improve the cycle performance of submicrometer-sized Si electrode, a composite conductive polymer binder composed of PPQ and PAA is adopted. Cycle performance of the electrode with submicrometer-sized Si powder with PPQ (30 wt.%) was very poor, capacity dropped at the first cycle. Cycle performance of the electrode is improved compare to the pristine electrode by means of compensation of poor adhesion strength of PPQ by adhesive PAA. Among the various composition of PPQ and PAA, QA21 in which PPQ content is highest showed most stable cycle performance. While the adhesion strength of the electrode increased as PAA ratio is increased in the composite binder, internal resistance of the electrode was increase to bring capacity fading, which is due to lack of PPQ conductive binder that plays a role of conductive additive. In addition, compared

with use of conventional super-P carbon black conductive additive, use of PPQ as a polymeric conductive additive brings more stable cycle performance of the submicrometer-sized Si electrode.

Finally, in the condition of high rate discharging, Li^+ ion conductive binder, LiPAA, lowers polarization to Li^+ ion transfer in the interface between the active material and the electrolyte. Li^+ ion accessible sites in the surface of the $LiFePO_4$ particle are wider in case of the LiPAA binder. Due to the difficulty in the migration of Li^+ ions through the surfaces covered with the PAA binder, high rate discharge of the $LiFePO_4$ electrode with the PAA is limited. In contrast, because Li^+ ions can migrate through the LiPAA binder layer, charge transfer resistance becomes lowered and discharge rate capability of the electrode with the LiPAA binder is better than that with the PAA binder.

5. References

[1] M. S. Whittingham, *Science*, 1976, **192**, 1126-1127.

[2] M. S. Whittingham, *Prog. Solid State Chem.*, 1978, **12**, 41-99.

[3] M. S. Whittingham*, United States Patent,* 4009052, 1977.

[4] M. Lazzari and B. Scrosati, *J. Electrochem. Soc.*, 1980, **127**, 773-774.

[5] D. W. Murphy, F. J. Di Salvo, J. N. Carides and J. V. Waszczak, *Mater. Res. Bull.*, 1978, **13**, 1395-1402.

[6] D. MacArthur, in *Lithium Batteries: Science and Technology*, eds. G.-A. Nazri and G. Pistoia, Springer, 2009, pp. 701-706.

[7] P. Kurzweil and K. Brandt, in *Encyclopedia of Electrochemical Power Sources*, ed. G. Editor-in-Chief: Jürgen, Elsevier, Amsterdam, 2009, pp. 1-26.

[8] J. M. Tarascon and M. Armand, *Nature*, 2001, **414**, 359-367.

[9] K. Mizushima, P. C. Jones, P. J. Wiseman and J. B. Goodenough, *Mater. Res. Bull.*, 1980, **15**, 783-789.

[10] M. M. Thackeray, W. I. F. David, P. G. Bruce and J. B. Goodenough, *Mater. Res. Bull.*, 1983, **18**, 461-472.

[11] M. M. Thackeray, P. J. Johnson, L. A. de Picciotto, P. G. Bruce and J. B. Goodenough, *Mater. Res. Bull.*, 1984, **19**, 179-187.

[12] R. Fong, U. von Sacken and J. R. Dahn, *J. Electrochem. Soc.*, 1990, **137**, 2009-2013.

[13] A. Kominato, E. Yasukawa, N. Sato, T. Ijuuin, H. Asahina and S. Mori, *J. Power Sources*, 1997, **68**, 471-475.

[14] S. Mori, H. Asahina, H. Suzuki, A. Yonei and K. Yokoto, *J. Power Sources*,

1997, **68**, 59-64.

[15] Y. Wang, S. Nakamura, M. Ue and P. B. Balbuena, *J. Am. Chem. Soc.*, 2001, **123**, 11708-11718.

[16] G. G. Amatucci, J. M. Tarascon and L. C. Klein, *J. Electrochem. Soc.*, 1996, **143**, 1114-1123.

[17] D. Aurbach, B. Markovsky, A. Rodkin, E. Levi, Y. S. Cohen, H. J. Kim and M. Schmidt, *Electrochim. Acta*, 2002, **47**, 4291-4306.

[18] A. Van der Ven, M. K. Aydinol and G. Ceder, *J. Electrochem. Soc.*, 1998, **145**, 2149-2155.

[19] J. P. Peres, C. Delmas, A. Rougier, M. Broussely, F. Perton, P. Biensan and P. Willmann, *J. Phys. Chem. Solids*, 1996, **57**, 1057-1060.

[20] S. Albrecht, J. Kümpers, M. Kruft, S. Malcus, C. Vogler, M. Wahl and M. Wohlfahrt-Mehrens, *J. Power Sources*, 2003, **119–121**, 178-183.

[21] C. H. Chen, J. Liu, M. E. Stoll, G. Henriksen, D. R. Vissers and K. Amine, *J. Power Sources*, 2004, **128**, 278-285.

[22] K. Y. Chung and K.-B. Kim *J. Electrochem. Soc.*, 2002, **149**, A79-A85.

[23] D. H. Jang, Y. J. Shin and S. M. Oh, *J. Electrochem. Soc.*, 1996, **143**, 2204-2211.

[24] M. M. Thackeray, Y. Shao-Horn, A. J. Kahaian, K. D. Kepler, E. Skinner, J. T. Vaughey and S. A. Hackney, *Electrochem. Solid-State Lett.*, 1998, **1**, 7-9.

[25] Y. Xia, Y. Zhou and M. Yoshio, *J. Electrochem. Soc.*, 1997, **144**, 2593-2600.

[26] S. Mandal, R. M. Rojas, J. M. Amarilla, P. Calle, N. V. Kosova, V. F. Anufrienko and J. M. Rojo, *Chem. Mater.*, 2002, **14**, 1598-1605.

[27] S.-T. Myung, S. Komaba and N. Kumagai, *J. Electrochem. Soc.*, 2001, **148**, A482-A489.

[28] R. Thirunakaran, N. Kalaiselvi, P. Periasamy, B. R. Babu, N. G. Renganathan,

N. Muniyandi and M. Raghavan, *Ionics*, **7**, 187-191.

[29] J. Cho, Y. J. Kim, T.-J. Kim and B. Park, *Chem. Mater.*, 2001, **13**, 18-20.

[30] J. Cho, Y.-W. Kim, B. Kim, J.-G. Lee and B. Park, *Angew. Chem.-Int. Edit.*, 2003, **42**, 1618-1621.

[31] A. K. Padhi, K. S. Nanjundaswamy and J. B. Goodenough, *J. Electrochem. Soc.*, 1997, **144**, 1188-1194.

[32] A. K. Padhi, K. S. Nanjundaswamy, C. Masquelier, S. Okada and J. B. Goodenough, *J. Electrochem. Soc.*, 1997, **144**, 1609-1613.

[33] J. Wang and X. Sun, *Energy Environ. Sci.*, 2012, **5**, 5163-5185.

[34] W.-J. Zhang, *J. Power Sources*, 2011, **196**, 2962-2970.

[35] *Principles and Applications of Lithium Secondary Batteries*, Wiley-VCH Verlag GmbH & Co. KGaA, 2012.

[36] C. Delacourt, P. Poizot, S. Levasseur and C. Masquelier, *Electrochem. Solid-State Lett.*, 2006, **9**, A352-A355.

[37] B. Einhorn and H. Kim, *Samsung and LG Have a Battery Problem: China has cut subsidies for the Korean companies' models*, Bloomberg Businessweek, April 1, 2016, (http://www.bloomberg.com/news/articles/2016-03-31/samsung-and-lg-have-a-battery-problem)

[38] D. Guerard and A. Herold, *Carbon*, 1975, **13**, 337-345.

[39] T. Ohzuku, Y. Iwakoshi and K. Sawai, *J. Electrochem. Soc.*, 1993, **140**, 2490-2498.

[40] J. R. Dahn, T. Zheng, Y. Liu and J. S. Xue, *Science*, 1995, **270**, 590-593.

[41] A. Mabuchi, K. Tokumitsu, H. Fujimoto and T. Kasuh, *J. Electrochem. Soc.*, 1995, **142**, 1041-1046.

[42] M. Winter, J. O. Besenhard, M. E. Spahr and P. Novák, *Adv. Mater.*, 1998, **10**, 725-763.

[43] A. Yoshino, The Past, Present and Future of the Lithium Ion Battery, https://www.natureasia.com/en/advertising/tech-forum/reports/01-materials-sep-24, (accessed 12 April, 2016).

[44] A. N. Dey, *J. Electrochem. Soc.*, 1971, **118**, 1547-1549.

[45] H. Wu and Y. Cui, *Nano Today*, 2012, **7**, 414-429.

[46] H. Li, X. Huang, L. Chen, Z. Wu and Y. Liang, *Electrochem. Solid-State Lett.*, 1999, **2**, 547-549.

[47] B. Laïk, L. Eude, J.-P. Pereira-Ramos, C. S. Cojocaru, D. Pribat and E. Rouvière, *Electrochim. Acta*, 2008, **53**, 5528-5532.

[48] K. Peng, J. Jie, W. Zhang and S.-T. Lee, *Appl. Phys. Lett.*, 2008, **93**, 033105.

[49] K. W. Kim, H. Park, J. G. Lee, J. Kim, Y.-U. Kim, J. H. Ryu, J. J. Kim and S. M. Oh, *Electrochim. Acta*, 2013, **103**, 226-230.

[50] T. Kim, S. Park and S. M. Oh, *J. Electrochem. Soc.*, 2007, **154**, A1112-A1117.

[51] S. Chen, M. L. Gordin, R. Yi, G. Howlett, H. Sohn and D. Wang, *PCCP*, 2012, **14**, 12741-12745.

[52] S. Iwamura, H. Nishihara and T. Kyotani, *J. Phys. Chem. C*, 2012, **116**, 6004-6011.

[53] H. Wu, G. Zheng, N. Liu, T. J. Carney, Y. Yang and Y. Cui, *Nano Lett.*, 2012, **12**, 904-909.

[54] Z. Y. Zeng, J. P. Tu, Y. Z. Yang, J. Y. Xiang, X. H. Huang, F. Mao and M. Ma, *Electrochim. Acta*, 2008, **53**, 2724-2728.

[55] X. N. Zhang, G. L. Pan, G. R. Li, J. Q. Qu and X. P. Gao, *Solid State Ionics*, 2007, **178**, 1107-1112.

[56] P. Zuo and G. Yin, *J. Alloys Compd.*, 2006, **414**, 265-268.

[57] A. Nagai, in *Lithium-Ion Batteries*, eds. M. Yoshio, R. J. Brodd and A. Kozawa, 2009, pp. 155-161.

[58] J.-P. Yen, C.-M. Lee, T.-L. Wu, H.-C. Wu, C.-Y. Su, N.-L. Wu and J.-L. Hong, *ECS Electrochemistry Letters*, 2012, **1**, A80-A82.

[59] J. Drofenik, M. Gaberscek, R. Dominko, F. W. Poulsen, M. Mogensen, S. Pejovnik and J. Jamnik, *Electrochim. Acta*, 2003, **48**, 883-889.

[60] J.-H. Lee, U. Paik, V. A. Hackley and Y.-M. Choi, *J. Electrochem. Soc.*, 2005, **152**, A1763-A1769.

[61] J. Li, R. B. Lewis and J. R. Dahn, *Electrochem. Solid-State Lett.*, 2007, **10**, A17-A20.

[62] B. Lestriez, S. Bahri, I. Sandu, L. Roué and D. Guyomard, *Electrochem. Commun.*, 2007, **9**, 2801-2806.

[63] J. S. Bridel, T. Azaïs, M. Morcrette, J. M. Tarascon and D. Larcher, *Chem. Mater.*, 2010, **22**, 1229-1241.

[64] J.-S. Bridel, T. Azaïs, M. Morcrette, J.-M. Tarascon and D. Larcher, *J. Electrochem. Soc.*, 2011, **158**, A750-A759.

[65] A. Magasinski, B. Zdyrko, I. Kovalenko, B. Hertzberg, R. Burtovyy, C. F. Huebner, T. F. Fuller, I. Luzinov and G. Yushin, *ACS Appl. Mater. Interfaces*, 2010, **2**, 3004-3010.

[66] S. Komaba, K. Shimomura, N. Yabuuchi, T. Ozeki, H. Yui and K. Konno, *J. Phys. Chem. C*, 2011, **115**, 13487-13495.

[67] S. Komaba, T. Ozeki, N. Yabuuchi and K. Shimomura, *Electrochemistry*, 2011, **79**, 6-9.

[68] I. Kovalenko, B. Zdyrko, A. Magasinski, B. Hertzberg, Z. Milicev, R. Burtovyy, I. Luzinov and G. Yushin, *Science*, 2011, **334**, 75-79.

[69] M. K. Dufficy, S. A. Khan and P. S. Fedkiw, *Journal of Materials Chemistry A*, 2015, **3**, 12023-12030.

[70] K. Prasanna, T. Subburaj, Y. N. Jo, W. J. Lee and C. W. Lee, *ACS Appl. Mater.*

Interfaces, 2015, **7**, 7884-7890.

[71] M. Murase, N. Yabuuchi, Z.-J. Han, J.-Y. Son, Y.-T. Cui, H. Oji and S. Komaba, *ChemSusChem*, 2012, **5**, 2307-2311.

[72] C.-C. Li and Y.-W. Wang, *J. Electrochem. Soc.*, 2011, **158**, A1361-A1370.

[73] Z. P. Cai, Y. Liang, W. S. Li, L. D. Xing and Y. H. Liao, *J. Power Sources*, 2009, **189**, 547-551.

[74] Z. Zhang, T. Zeng, C. Qu, H. Lu, M. Jia, Y. Lai and J. Li, *Electrochim. Acta*, 2012, **80**, 440-444.

[75] A. Guerfi, M. Kaneko, M. Petitclerc, M. Mori and K. Zaghib, *J. Power Sources*, 2007, **163**, 1047-1052.

[76] N. P. W. Pieczonka, V. Borgel, B. Ziv, N. Leifer, V. Dargel, D. Aurbach, J.-H. Kim, Z. Liu, X. Huang, S. A. Krachkovskiy, G. R. Goward, I. Halalay, B. R. Powell and A. Manthiram, *Advanced Energy Materials*, 2015, **5**, 1501008.

[77] S.-L. Chou, Y. Pan, J.-Z. Wang, H.-K. Liu and S.-X. Dou, *PCCP*, 2014, **16**, 20347-20359.

[78] Z. P. Guo, J. Z. Wang, H. K. Liu and S. X. Dou, *J. Power Sources*, 2005, **146**, 448-451.

[79] Y. Wang, Y. Wang, E. Hosono, K. Wang and H. Zhou, *Angew. Chem.-Int. Edit.*, 2008, **47**, 7461-7465.

[80] J.-M. Kim, H.-S. Park, J.-H. Park, T.-H. Kim, H.-K. Song and S.-Y. Lee, *ACS Appl. Mater. Interfaces*, 2014, **6**, 12789-12797.

[81] T. M. Higgins, S.-H. Park, P. J. King, C. Zhang, N. McEvoy, N. C. Berner, D. Daly, A. Shmeliov, U. Khan, G. Duesberg, V. Nicolosi and J. N. Coleman, *ACS Nano*, 2016, **10**, 3702-3713.

[82] G. Liu, S. Xun, N. Vukmirovic, X. Song, P. Olalde-Velasco, H. Zheng, V. S. Battaglia, L. Wang and W. Yang, *Adv. Mater.*, 2011, **23**, 4679-4683.

[83] C. Wang, A. J. Appleby and F. E. Little, *J. Electroanal. Chem.*, 2001, **497**, 33-46.

[84] M. N. Obrovac and L. J. Krause, *J. Electrochem. Soc.*, 2007, **154**, A103-A108.

[85] M. N. Obrovac and L. Christensen, *Electrochem. Solid-State Lett.*, 2004, **7**, A93-A96.

[86] T. D. Hatchard and J. R. Dahn, *J. Electrochem. Soc.*, 2004, **151**, A838-A842.

[87] T. Takamura, S. Ohara, M. Uehara, J. Suzuki and K. Sekine, *J. Power Sources*, 2004, **129**, 96-100.

[88] H. Kim, M. Seo, M.-H. Park and J. Cho, *Angew. Chem.-Int. Edit.*, 2010, **49**, 2146-2149.

[89] J.-H. Kim, H.-J. Sohn, H. Kim, G. Jeong and W. Choi, *J. Power Sources*, 2007, **170**, 456-459.

[90] M. Winter and J. O. Besenhard, *Electrochim. Acta*, 1999, **45**, 31-50.

[91] P. Novák, K. Müller, K. S. V. Santhanam and O. Haas, *Chem. Rev.*, 1997, **97**, 207-282.

[92] S.-M. Kim, M. H. Kim, S. Y. Choi, J. G. Lee, J. Jang, J. B. Lee, J. H. Ryu, S. S. Hwang, J.-H. Park, K. Shin, Y. G. Kim and S. M. Oh, *Energy Environ. Sci.*, 2015, **8**, 1538-1543.

[93] C. Yang, H. Scheiber, E. J. W. List, J. Jacob and K. Müllen, *Macromolecules*, 2006, **39**, 5213-5221.

[94] W. Vanormelingen, A. Smeets, E. Franz, I. Asselberghs, K. Clays, T. Verbiest and G. Koeckelberghs, *Macromolecules*, 2009, **42**, 4282-4287.

[95] J. H. Ryu, J. W. Kim, Y.-E. Sung and S. M. Oh, *Electrochem. Solid-State Lett.*, 2004, **7**, A306-A309.

[96] M. Wu, X. Xiao, N. Vukmirovic, S. Xun, P. K. Das, X. Song, P. Olalde-Velasco, D. Wang, A. Z. Weber, L.-W. Wang, V. S. Battaglia, W. Yang and G. Liu, *J.*

Am. Chem. Soc., 2013, **135**, 12048-12056.

[97] E. Pollak, G. Salitra, V. Baranchugov and D. Aurbach, *J. Phys. Chem. C*, 2007, **111**, 11437-11444.

[98] H. Park, T. Yoon, Y.-U. Kim, J. H. Ryu and S. M. Oh, *Electrochim. Acta*, 2013, **108**, 591-595.

[99] S. Komaba, K. Okushi, T. Ozeki, H. Yui, Y. Katayama, T. Miura, T. Saito and H. Groult, *Electrochem. Solid-State Lett.*, 2009, **12**, A107-A110.

[100] D. Lin, Z. Lu, P.-C. Hsu, H. R. Lee, N. Liu, J. Zhao, H. Wang, C. Liu and Y. Cui, *Energy Environ. Sci.*, 2015, **8**, 2371-2376.

[101] Z. Chen and J. R. Dahn, *J. Electrochem. Soc.*, 2002, **149**, A1184-A1189.

[102] W.-R. Liu, Z.-Z. Guo, W.-S. Young, D.-T. Shieh, H.-C. Wu, M.-H. Yang and N.-L. Wu, *J. Power Sources*, 2005, **140**, 139-144.

[103] J. S. Bridel, T. Azaïs, M. Morcrette, J. M. Tarascon and D. Larcher, *Chem. Mater.*, 2010, **22**, 1229-1241.

[104] J. G. Lee, J. Kim, H. Park, J. B. Lee, J. H. Ryu, J. J. Kim and S. M. Oh, *J. Electrochem. Soc.*, 2015, **162**, A1579-A1584.

[105] D. Shao, H. Zhong and L. Zhang, *ChemElectroChem*, 2014, **1**, 1679-1687.

[106] Z. Zhang, Z. Zhang, W. Chen, G. Wang, J. Li and Y. Lai, *New J. Chem.*, 2015, **39**, 3765-3769.

[107] R. Dominko, M. Bele, M. Gaberscek, M. Remskar, D. Hanzel, S. Pejovnik and J. Jamnik, *J. Electrochem. Soc.*, 2005, **152**, A607-A610.

[108] J. Chong, S. Xun, H. Zheng, X. Song, G. Liu, P. Ridgway, J. Q. Wang and V. S. Battaglia, *J. Power Sources*, 2011, **196**, 7707-7714.

[109] Z. Chen, L. Christensen and J. R. Dahn, *J. Appl. Polym. Sci.*, 2004, **91**, 2958-2965.

[110] A. Chapiro, Z. Mankowski and N. Schmitt, *Journal of Polymer Science:*

Polymer Chemistry Edition, 1982, **20**, 1791-1796.

[111] K. Terao, in *Encyclopedia of Polymeric Nanomaterials*, eds. S. Kobayashi and K. Müllen, Springer Berlin Heidelberg, Berlin, Heidelberg, 2014, pp. 1-6.

[112] E. S. Rufino and E. E. C. Monteiro, *Polymer*, 2000, **41**, 4213-4222.

[113] B. Basnar, S. Schartner, M. Austerer, A. M. Andrews, T. Roch, W. Schrenk and G. Strasser, *Opt. Express*, 2008, **16**, 8557-8569.

[114] T. R. Jow, M. B. Marx and J. L. Allen, *J. Electrochem. Soc.*, 2012, **159**, A604-A612.

[115] S. Komaba, N. Yabuuchi, T. Ozeki, K. Okushi, H. Yui, K. Konno, Y. Katayama and T. Miura, *J. Power Sources*, 2010, **195**, 6069-6074.

요약(국문초록)

리튬 이온 전지용 전자/이온 전도성 고분자 바인더: 폴리페난트렌퀴논 및 폴리아크릴산 리튬염

김 상 모

서울대학교 대학원

화학생물공학부

리튬 이온 전지 전극을 이루는 구성요소 중 바인더는 활물질과 도전재와 집전체를 결합하여 전극 내에서 전기화학 반응이 잘 일어날 수 있도록 돕는 물질이다. Polyvinylidene fluoride (PVDF)는 화학적, 전기화학적 안정성이 우수하여 지금까지 리튬 이온 전지에 널리 사용되었지만 고용량, 고출력 성능을 가지는 활물질에 대한 연구가 증가함에 따라 해당 성능을 뒷받침 해줄 수 있는 기능성 바인더에 대한 연구가 활발히 진행되고 있다. 본 연구에서는 고용량 Si 음극과 고출력 $LiFePO_4$ 양극에 응용될 수 있는 전자/이온 전도성 고분자 바인더의 전기화학적 특성에 대해 알아보았다.

Si은 이론용량이 3579 mA h g^{-1}에 달해 흑연을 대체할 차세대 음극 활물질로 주목을 받고 있지만 충방전 시 약 300배의 부피 변화가 일어나기 때문에 결착력이 약한 기존 PVDF 바인더를 대신해 결착력이 좋은 carboxymethyl cellulose (CMC)나 poly(acrylic acid) (PAA)같은

카복시기를 가지는 고분자 바인더 사용이 검토되고 있다. 이와 함께 벌크 크기 입자에 비해 부피 변화 효과가 작은 나노 크기의 Si 입자를 사용할 경우 우수한 수명 특성을 얻을 수 있다. 하지만 큰 비표면적으로 인해 전극 슬러리 제조 공정에서 분산에 문제가 있으며 전극의 전기적 네트워크 향상을 위해 많은 양의 도전재와 바인더가 사용되어야 한다. 이 경우 전체 전극의 에너지 밀도를 저하시키는 문제가 발생한다.

나노 크기의 Si 분말의 상업적 이용에 대한 가능성 향상을 위해 도전재를 대체하는 페난트렌퀴논(phenanthrenequinone) 기반의 전도성 고분자 바인더(PPQ)에 대한 연구를 수행하였다. 해당 고분자는 Si의 첫 사이클에서의 충전 반응 이전에 환원(n-도핑)되어 mixed conductor가 되고 Si의 방전 종지전압에서도 도핑된 상태를 유지하는 것을 확인하였다. 도전재를 사용하지 않고 제조한 Si 전극의 속도 특성을 비전도성 바인더를 사용한 전극과 비교하였을 때 월등히 우수한 속도 특성을 보였다. Galvanostatic intermittent titration technique (GITT)를 통해 충방전 시 전극의 내부저항을 계산한 결과, PPQ 전도성 고분자 바인더를 사용한 전극에서 저항이 더 작음을 확인하였다. 이는 PPQ 고분자 바인더가 Si 입자 표면에 균일하게 분포함으로써 Si 입자와 입자 사이 또는 Si 입자와 구리 집전체 사이에서 전자를 원활히 이동시켜주기 때문이다. 다시 말해 PPQ 전도성 고분자가 도전재로서 역할을 한다고 할 수 있다.

나노 크기의 Si 분말은 전극 제조 공정 상 균일한 분산이 어려운 문제가 있고 큰 비표면적으로 인한 입자간 반발력으로 탭밀도가 저하되는 문제가 있다. 이를 위해 마이크로미터 크기의 입자의 활용이 검토될 수 있다. 마이크로크기의 Si 입자를 볼밀을 통해 1 μm 이하의 크기를 가진 입자로

만들어 주었고 더 커진 부피변화를 감당하기 위해 결착력이 좋은 바인더인 PAA를 첨가하였다. 도전재를 사용하지 않고, 볼밀한 Si과 PPQ만을 사용해서 제조한 전극의 결착력은 0.06 N cm^{-1}이었지만 PAA를 전체 바인더 무게 대비 33 % 첨가했을 때 약 2 N cm^{-1}로 30배 정도 향상됨을 확인하였다. 이에 따라 Si 전극의 수명 특성도 월등히 향상되었음을 확인하였다. PPQ와 PAA가 복합체를 이루면서 PPQ는 전자를 이동시켜 주는 도전재 역할을, PAA는 Si 부피 변화 시 전극을 결합해주는 역할을 함을 알 수 있다.

$LiFePO_4$의 고속 충방전 시 발생하는 분극을 감소시키기 위해 활물질 입자 표면을 탄소로 코팅하여 전자의 흐름을 원활히 해준다. 하지만 활물질과 전해질 사이의 계면에서의 빠른 전기화학반응에서 리튬 이온 전달 저항에 의해 분극이 발생하기도 한다. 리튬 이온을 전달할 수 있는 바인더의 효과를 알아보기 위해 poly(acrylic acid) lithium salt (LiPAA)를 사용하였고, 리튬 이온을 전달하기 어려운 PAA 바인더와 비교하여 전기화학적 특성을 분석하였다. LiPAA 바인더를 사용한 $LiFePO_4$ 전극의 고율에서의 방전 용량이 PAA를 사용한 전극보다 더 큼을 확인하였고 3.34 V (*vs.* Li/Li^+)에서 보이는 방전 전압 평탄부에 걸리는 분극도 더 작음을 확인하였다. LiPAA와 PAA로 필름을 제조한 후 리튬 금속 대칭 셀(symmetrical cell)을 구성하여 galvanostatic polarization 실험을 수행한 결과 LiPAA 필름에서 리튬 이온 전달에 의한 분극이 훨씬 작게 걸리는 것을 확인하였다. 또한 충전 상태의 $LiFePO_4$ 전극으로 대칭 셀을 구성하고 전기화학 임피던스 실험을 수행한 결과 LiPAA로 제조한 전극의 전하 전달 저항이 PAA를 사용한 전극보다 더 작음을 확인하였다. 이는 LiPAA의

carboxylate 음이온이 PAA의 카복시기보다 리튬 이온에 대한 친화성이 더 높으므로 고속 방전 상황에서 활물질 표면에 존재하는 LiPAA 바인더를 통한 전하 전달이 더 용이해, 더 나은 출력 특성을 나타낸다고 설명할 수 있다.

……

주요어: 리튬 이온 전지, 전자 전도성 바인더, 리튬이온 전도성 바인더, 실리콘 음극, $LiFePO_4$ 양극, 폴리페난트렌퀴논, 폴리아크릴산

학 번: 2010-31324